Journal of Aerosol Science 96 (2016) 69–95

Contents lists available at ScienceDirect

Journal of Aerosol Science

journal homepage: www.elsevier.com/locate/jaerosci

Three-dimensional motion of particles in a shear flow near a rough wall

F. Feuillebois [a], F. Gensdarmes [b,*], Z. Mana [b,c,e], L. Ricciardi [b], C. Monier [c], G. Le Meur [c], C. Reynaud [d], M. Rabaud [e]

[a] 2 allée des Mouilleboeufs, 92350 Le Plessis Robinson, France
[b] Institut de Radioprotection et de Sûreté Nucléaire (IRSN), Gif-sur-Yvette 91192, France
[c] Électricité de France, EDF R& D, Chatou 78401, France
[d] BIOPHY RESEARCH S.A., Actipôle St Charles, 131 Avenue de l'Étoile, 13710 Fuveau, France
[e] Laboratoire FAST, Université Paris-Sud, CNRS, Université Paris-Saclay, F-91405 Orsay, France

ARTICLE INFO

Article history:
Received 1 July 2015
Received in revised form
16 October 2015
Accepted 20 October 2015
Available online 17 November 2015

Keywords:
Solid particles
Rough wall
Adhesion force
Shear flow
Entrainment
3D trajectories

ABSTRACT

A model is proposed for the three-dimensional motion of a small spherical particle entrained by the shear flow of a gas near a rough wall. On the basis of experimental results, the wall is modeled by an average small roughness and some much larger isolated peaks, which are yet smaller than the sphere radius. When encountering a high peak of roughness, the particle may be lifted if the aerodynamic force and torque take over the force and torque due to adhesion on the wall. The aerodynamics is treated using previous analytical results for the creeping flow around a particle near a wall. Values of the adhesion forces of a particle near a rough wall are obtained experimentally. When lifted from the wall, the particle follows a three-dimensional trajectory while rotating around the peak of roughness. Examples of calculated trajectories show that the particle may or may not reach the top of the peak, depending on the various physical parameters. Since the velocity of the particle when leaving the peak grows with its final distance from the wall, that velocity is essential for the subsequent particle resuspension by the ambient shear flow.

1. Introduction

In nuclear facilities, during normal operations in controlled areas, workers might be exposed to radioactive aerosols. Potential sources of airborne contamination are particles that are initially spread on the floor and later removed by walking workers. Particle resuspension by walking on a contaminated soil may be due either to the airflow blown by the shoe motion or to the mechanical action of the shoe. At present, studies on this topic are sparse and only empirical relationships are available (Jones & Pond, 1964; Brunskill, 1964; Boulaud et al., 2003). In order to assess occupational exposure and define the most appropriate protections for the workers, it is suitable to determine the particle resuspension rate for new situations. Empirical considerations may then not be sufficient and consequently modeling is needed (Mana, 2014).

Furthermore, there is a strong interest in the scientific community for this type of problem, especially in the framework of air quality in domestic environment (Gomes, Freihaut, & Bahnfleth, 2007; Qian & Ferro, 2008; Rosati, Thornburg, & Rodes,

* Corresponding author.
E-mail addresses: francois.feuillebois@yahoo.fr (F. Feuillebois), francois.gensdarmes@irsn.fr (F. Gensdarmes).

http://dx.doi.org/10.1016/j.jaerosci.2015.10.004
0021-8502/

Nomenclature

a	radius of spherical particle (m)
$\mathbf{C}$	aerodynamic torque on particle (N.m)
c	(with indices) friction factor for torque $\mathbf{C}$ (dimensionless)
$(\mathbf{e}_1, \mathbf{e}_2, \mathbf{e}_3)$	base vectors of the (x_1, x_2, x_3) frame (dimensionless)
E_1, E_2	Young moduli of materials 1, 2 (Pa)
f	(with indices) friction factor for force $\mathbf{F}$ (dimensionless)
$\mathbf{F}$	aerodynamic force on particle (N)
H	center of circular region of contact of the spherical particle with the rough wall
H'	projection of the sphere center O onto the base plane
$\mathbf{H}$	reaction force of rough wall onto particle at point H (N)
I	moment of inertia of particle (kg m^2)
$\mathcal{I}$	impact factor (dimensionless)
$(\mathbf{i}, \mathbf{j}, \mathbf{k})$	base vectors of (x, y, z) frame (dimensionless)
k_q	constant coefficient of quadratic shear flow (m^{-1} s^{-1})
k_s	constant coefficient of linear shear flow (s^{-1})
$\widetilde{k}_q$	normalized ratio ak_q/k_s (dimensionless)
ℓ	distance between sphere center and base plane (m)
m	mass of particle (kg)
$\mathbf{n}$	unit vector normal to sphere at peak P (dimensionless)
O	sphere center
P	peak of roughness
P'	projection of P onto base plane
$\mathbf{P}$	reaction force of peak P onto particle (N)
r_c	contact radius of deformed elastic spherical particle
$\widetilde{r}_c$	r_c/a (dimensionless)
$\mathfrak{R}$	Reynolds number (dimensionless)
S_{tk}	Stokes number (dimensionless)
t	time (s)
$\widetilde{t}$	dimensionless time $k_s t$
$\mathbf{U}$	sphere translational velocity (m/s)
U_x	x component of $\mathbf{U}$
$\widetilde{U}_x$	$U_x/(ak_s)$ (dimensionless)
$\mathbf{v}_\infty$	ambient flow velocity (m/s)
V_s	stokes velocity of particle submitted to force $\mathbf{W}$ (m/s)
$\widetilde{V}_s$	normalized Stokes velocity $V_s/(ak_s)$ (dimensionless)
$\mathbf{W}$	weight plus adhesion force, normal to wall (N)
$\mathbf{W}_A$	adhesion force (N)
(x, y, z)	cartesian frame of coordinates attached to the wall and with origin specified in Section 5.2 (m)
$\mathbf{x}$	position vector in frame (x, y, z) (m)
(x_1, x_2, x_3)	cartesian frame of coordinates attached to the wall and with origin at point H' at time t (m)
(X, Y, Z)	coordinates of sphere center O in frame (x, y, z) (m)

Greek letters

β	distance of P' from origin of (x, y, z) frame
δ	distance of peak P from base plane
Φ	value of angle ϕ for non-lifted sphere
ε	gap between base plane and particle surface (dimensionless)
θ	angle between axes x and x_1
μ	gas dynamic viscosity (Pa s)
μ_s, μ_d	static and dynamic solid friction factors (dimensionless)
ν	gas kinematic viscosity (m^2/s)
ν_1, ν_2	Poisson coefficients of materials 1, 2 (dimensionless)
ρ_a	air density (kg/m^3)
ρ_p	particle density (kg/m^3)
τ_p	particle relaxation time (s)
ϕ	angle $\widehat{HOP}$ between center H of contact region and peak P, as viewed from sphere center O
ψ	angle of rotation around axis x_1
$\mathbf{\Omega}$	sphere rotational velocity (s^{-1})
Ω_y	y component of $\mathbf{\Omega}$ (s^{-1})
$\widetilde{\Omega}_y$	Ω_y/k_s (dimensionless)

Superscripts

$(\,)^t$	translation
$(\,)^r$	rotation
$(\,)^s$	linear shear flow
$(\,)^q$	quadratic shear flow

Subscripts

O	refers to sphere center O
P	refers to peak P
$(\,)_x, (\,)_y, (\,)_z$	components in frame (x, y, z)
$(\,)_1, (\,)_2, (\,)_3$	components in frame (x_1, x_2, x_3)

2008; Oberoi et al., 2010; Choi, Edwards, Rosati, & Eisner, 2012; Kubota & Higuchi, 2013). All these studies show that obviously particle size is a critical parameter in the resuspension phenomenon and that soil characteristics (hard surface, roughness, new or worn carpet) are also relevant.

Analytical models describing the resuspension of micron-sized particles by an airflow generally consider that the characteristic scale of the surface roughness is small compared with the diameter of the particle (Reeks & Hall, 2001; Ibrahim, Dunn, & Brach, 2003; Goldasteh, Goodarz, & Ferro, 2013; Zhang, Reeks, & Kissane, 2013). In this case, the particle has several contact points with the asperities of the surface. The analysis of its motion is simplified by performing a balance of the moments of forces along two dimensions in a plane parallel to the direction of airflow. The role of surface roughness,

including the presence of asperities at small or large scales compared with the particle size, was investigated by Guingo & Minier (2008). The authors show the importance of a complete description of the surface roughness at different scales in order to understand the adhesion and resuspension of particles. Their results prove that the time dependent resuspension rate does not vary in a monotonic way with the considered surface roughness scales. They explain that for a large scale roughness, that is when a particle is small compared with the distance between two peaks, it has to travel a variable distance before touching an asperity and rocking around it, thereby triggering its resuspension. Here again the authors use a balance of moments of forces in two dimensions to describe the detachment of particles. This modeling in two dimensions implies that if the particle is moved upwards, it is forced to pass through the top of the asperity. Therefore, since the particle is considered to be in a shear flow, it is submitted to a higher local velocity than if it would circumvent the asperity without reaching its top. That later consideration, that requires to be studied in three dimensions, is not included in current models and may have an impact on the final detachment behavior and particle resuspension.

We propose here a model for the three-dimensional motion of a micron size particle near a rough wall. In order to consider realistic parameters to achieve the calculations, we use the characteristics of a specific surface encountered in EDF nuclear facilities, which is a coating of epoxy resin on concrete. The topography of the surface is analyzed with a Atomic Force Microscope (AFM). In addition we use, as model input, measurements of adhesion forces of particles on the epoxy surface area. For this purpose, the particles of interest are stuck on the tip of a AFM cantilever. On the basis of these experimental results presented in an appendix, the wall is modeled by an average small roughness and some much larger isolated peaks, which are yet smaller than the sphere radius. In this model it is assumed that the particle, described as a perfect sphere, is initially deposited on the surface with a small roughness, and when moving along the wall comes in contact with a single large peak above the mean surface roughness. This peak is modeled as a single contact point with the sphere surface. From there, we describe the possible trajectories of the particle, depending on the particle diameter, height of asperity and initial position of the center of the particle with respect to the peak. The trajectories calculation takes into account the particle translational and rotational movements in three dimensions with and without slipping on the base rough wall. The perspective is to use this model in the calculation of the movement of particles on specific rough surfaces subjected to air shear flows generated by walking operators. Note that this problem may also have relevance to wet granular media (see e.g. Albert, Albert, Hornbaker, Schiffer, & Barabasi, 1997).

It is clear that the present model is limited to surfaces and particles for which a particle is in general in contact with a single high peak. Cases when a particle is in contact with two high peaks would need a special three-dimensional treatment, analogous to the one presented here. This is left for future studies.

The paper outline is as follows. A description of the model and underlying assumptions is presented in Section 2. Then, the problem notation, former results for the aerodynamic forces and torques and values of the adhesion force are presented in Section 3. The motion of a particle in contact with a rough wall is solved in Section 4, in the cases when the particle rolls without slip and with slip. For a particle in contact with a rough wall and a higher peak of roughness, Section 5, the problem appears to be undetermined; it is discussed in the cases of rolling without slip and with slip. Equations of the three-dimensional motion of a lifted particle rotating around a peak of roughness are presented in Section 6. Results of the calculation of the trajectories of the lifted particle are displayed in Section 7. Finally, the conclusion is in Section 8.

2. Model description and assumptions

Particles considered here are small and close to the wall, so that the flow in the vicinity of the wall is well approximated by a parabolic shear flow (see Section 3) and the Reynolds number of the flow around them is low compared with unity. Then, Stokes equations for fluid motion apply in the first approximation.

Note that Stokes equations for the fluid motion are steady, even though the particle motion is unsteady. This is because the characteristic time for motion of the particle is large compared with the time for diffusion of vorticity on the particle scale. Due to this “quasi-steady” flow, all unsteady forces like the added-mass and Boussinesq–Basset ones are negligible here (see Feuillebois, 1989).

Solutions of Stokes equations are well documented (see e.g. Happel & Brenner, 1973, for works until the 70s). In particular, there has been various results for the force and torque on a spherical particle near a plane wall when the no-slip boundary condition applies on both the particle and wall (see e.g. Feuillebois, 1989, for a review until the 80s). Among other results, the force and torque on a sphere in contact with a plane wall in a linear shear flow were calculated analytically using the method of tangent spheres coordinates by O'Neill (1968). Later on, following works by O'Neill and coworkers and by Goldman, Cox, & Brenner (1967), Chaoui & Feuillebois (2003) reconsidered the problem of the force and torque on a spherical particle translating and rotating in a linear shear flow close to a plane wall. They used the method of bispherical coordinates to find an analytical solution. An appropriate numerical technique was then applied to solve the resulting infinite linear systems with a large number of digits, leading to results with a 10^{-15} accuracy for the force and torque. These results are valid even for small gaps, down to 2×10^{-6} sphere radius, that is in the lubrication region. A similar approach was used by Pasol, Sellier, & Feuillebois (2006) to solve the problems of a spherical particle embedded in various ambient flow fields parallel to a plane wall, in particular a quadratic shear flow. All these results will be used in this paper.

Since fluid inertia is neglected, from the linearity of Stokes equations of fluid motion, a sphere in an ambient flow parallel to a wall is only submitted to a force along the wall (see Bretherton, 1962). That is, there is no lift force.

Even though fluid inertia is negligible, particle inertia may be significant because of the large density ratio between particle and air. That is, the *Stokes number* expressing particle inertia (see its definition, Eq. (9)) may be of order unity. This is important for particle trajectories.

Only spherical particles are considered here. Note that for non-spherical particles in a shear flow near a wall, the force and torque would be modified as calculated by Gavze and Shapiro (1997). Freely moving non-spherical particles in an unbounded shear flow rotate along *Jeffery orbits* and these orbits are modified when close to a wall as shown in Gavze and Shapiro (1998). If attached to a fixed point, it is also expected that a non-spherical particle would be submitted to a lift, even without fluid inertia.

The force and torque on a sphere moving in the normal direction to a rough wall is well described by taking into account an hypothetical equivalent smooth plane wall situated in the actual wall, at some distance of the order of the roughness from the top of the corrugations (Lecoq, Anthore, Cichocki, Szymczak, & Feuillebois, 2004; Vinogradova & Yakubov, 2006). This approach will be used here, in particular when the sphere is in the lubrication region. The equivalent smooth plane will be called the *base plane* here.

The mechanical problem of a spherical particle in contact with a rough wall in a viscous fluid may be modeled by simply superimposing the force and torque due to the fluid and those due to solid friction (see e.g. Bowden & Tabor, 1950). This model was validated, in the case of two rough spherical particles in contact, by experiments in which the sphere motion was measured accurately with laser interferometry (Ekiel-Jeżewska et al., 1999, Ekiel-Jeżewska, Lecoq, Anthore, Bostel, & Feuillebois, 2002). These experiments were performed with millimeter sized balls embedded in a very viscous oil. By Reynolds similitude, the conclusions apply to microscopic particles in water and also in a gas (in that case provided the considered distances are large compared with the mean free path). The regimes of rolling without slip and rolling with slip observed in experiments were well described by the model. Moreover, a conclusion is that the case of a rough sphere moving along another rough sphere at a small distance from it is well described by using the lubrication approximation with equivalent smooth spheres together with the simple Amonton–Coulomb's law for solid friction. That model from Ekiel-Jeżewska et al. (1999, 2002) will be used in this paper for a sphere moving in a gas along a rough wall.

Small particles on a rough wall are submitted to forces due to the ambient flow and to an adhesion force by this wall. It has been remarked that the adhesion force is widely decreased for a particle near a rough wall compared with a smooth wall (Cheng, Dunn, & Brach, 2002; Peressadko, Hosoda, & Persson, 2005). We will use here results from AFM measurements providing the wall roughness and values of the adhesion force which are well below those for a particle close to a smooth wall.

We consider here the scenarios of a spherical particle which may be lifted above a rough wall and then follows a three-dimensional trajectory in a gas flow. The particle is first in contact with a rough wall and moves along it, pushed by an ambient linear shear flow. At some point, the particle will encounter a roughness peak that is well higher than the average roughness. Then several scenarios may arise: the particle may rotate around the peak without leaving the base rough wall; for some values of physical parameters, the particle may be lifted and climb on the peak while rotating around it. Whether or not the particle will be lifted to the top of the peak also depends on the various parameters. Our purpose is to set up the equations of motion of the particle, apply the models of the forces and torques quoted above and solve for the possible particle trajectories of the lifted particle. Details of the models will be developed along the paper.

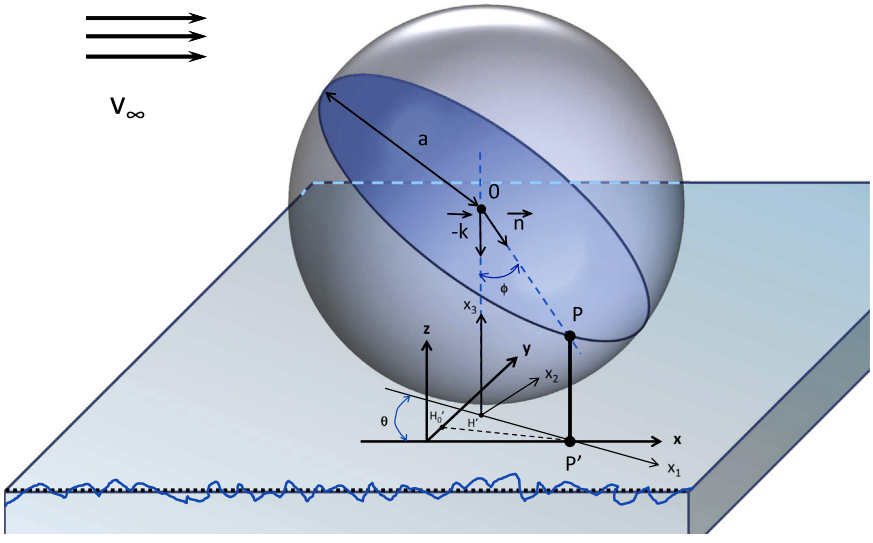

Fig. 1. Three-dimensional sketch of a spherical particle in contact with a rough wall and with a high peak of roughness represented as a point *P*. The point H' is the projection of the sphere center onto the base plane. The gap between H' and the sphere is of the order of the roughness height. The point H'_0 is the position of H' at time zero, when the sphere first hits the peak *P*.

3. Notation and forces

3.1. Notation

Consider a Cartesian coordinates system (x,y,z) with unit vectors $(\mathbf{i},\mathbf{j},\mathbf{k})$. The base plane is represented by $z=0$, see Fig. 1. Consider a gas flow along the wall, its velocity and pressure being described by:

$$\mathbf{v}_\infty = [k_s z + k_q z^2]\,\mathbf{i}, \quad p_\infty = 2\mu k_q x, \tag{1}$$

where $k_s z\mathbf{i}$ is a linear shear flow, $k_q z^2\,\mathbf{i}$ a quadratic shear flow (with constant coefficients k_s and k_q) and μ is the gas dynamic viscosity. The polynomial form (1) of the flow velocity may be considered as the first terms in a Taylor expansion of a more general velocity profile along the wall. Without loss of generality we assume here $k_s>0$. A characteristic Reynolds number based on the shear rate k_s and particle radius a is

$$\mathfrak{R} = \frac{k_s a^2}{\nu}, \tag{2}$$

where ν is the gas kinematic viscosity. This number is assumed to be low compared with unity.

The pressure gradient $\mathrm{d}p_\infty/\mathrm{d}x$ is in general negative for the gas to flow in the positive x direction, thus $k_q<0$. Moreover $|k_q|$ should be sufficiently small compared with k_s, so that $[k_s z + k_q z^2]>0$. Thus, at the scale a of a particle, the dimensionless quadratic shear rate

$$\widetilde{k}_q = \frac{a k_q}{k_s} \tag{3}$$

is usually small.

Consider a spherical particle with center O at position $\mathbf{x}_O=(X,Y,Z)$ at the considered time t. The particle moves with translational and rotational velocity

$$\mathbf{U} = \frac{\mathrm{d}\mathbf{x}_O}{\mathrm{d}t} = U_x\mathbf{i}+U_y\mathbf{j}+U_z\mathbf{k}, \quad \boldsymbol{\Omega} = \Omega_x\mathbf{i}+\Omega_y\mathbf{j}+\Omega_z\mathbf{k}. \tag{4}$$

The stresses due to the perturbed flow around the particle create an aerodynamic force and an aerodynamic torque

$$\mathbf{F} = F_x\mathbf{i}+F_y\mathbf{j}+F_z\mathbf{k}, \quad \mathbf{C} = C_x\mathbf{i}+C_y\mathbf{j}+C_z\mathbf{k}. \tag{5}$$

Details are given below in Section 3.2.

The particle is also submitted in the direction normal to the wall to a force $\mathbf{W}=-W\mathbf{k}$. This force may either be a weight for a large enough particle or an attractive adhesion force which acts only at a short distance, for a small particle. Here, we consider generally that $\mathbf{W}$ includes both the weight and adhesion. Details for the adhesion force are given below in Section 3.3.

A useful quantity for normalization is the instantaneous velocity of the spherical particle submitted to a force W when in unbounded fluid

$$V_s = \frac{W}{6\pi a\mu} \tag{6}$$

where $6\pi a\mu$ is the classical Stokes drag coefficient. The relaxation time for particle motion is

$$\tau_p = \frac{m}{6\pi a\mu} \tag{7}$$

where m is the particle mass. A characteristic time for the fluid motion is k_s^{-1}. The ratio of both characteristic times is the Stokes number

$$\mathrm{S_{tk}} = \tau_p k_s \tag{8}$$

which is representative for particle inertia in its motion when entrained by the gas. For a particle density ρ_p and a gas (say, air) with density ρ_a, (8) becomes with (2):

$$\mathrm{S_{tk}} = \frac{2}{9}\frac{\rho_p}{\rho_a}\,\mathfrak{R}. \tag{9}$$

Since the particle density is much larger than the gas density, the Stokes number $\mathrm{S_{tk}}$ may be large even though the Reynolds number $\mathfrak{R}$ is small.

3.2. Aerodynamic forces and torques

From $\mathfrak{R}\ll 1$, the flow at the particle scale satisfies in the first approximation the Stokes equations which are linear. Then, the various analytical results quoted in the introduction may be added by linearity.

Consider a spherical particle centered at a distance ℓ from a plane wall. By linearity of Stokes equations, the force and torque exerted by the flow field onto the translating and rotating particle in the ambient flow field (1) are obtained as sums

of forces and torques for elementary flow fields:

$$\mathbf{F} = \mathbf{F}^{\mathrm{t}} + \mathbf{F}^{\mathrm{r}} + \mathbf{F}^{\mathrm{s}} + \mathbf{F}^{\mathrm{q}}, \tag{10a}$$

$$\mathbf{C} = \mathbf{C}^{\mathrm{t}} + \mathbf{C}^{\mathrm{r}} + \mathbf{C}^{\mathrm{s}} + \mathbf{C}^{\mathrm{q}}, \tag{10b}$$

where the superscripts $(\,)^{\mathrm{t}}$ and $(\,)^{\mathrm{r}}$ stand respectively for the flow fields due to a translating and rotating particle in a fluid at rest; $(\,)^{\mathrm{s}}$ and $(\,)^{\mathrm{q}}$ stand for a particle held fixed in an ambient linear shear flow and quadratic shear flow, respectively.

Again by linearity of Stokes equations, the forces and torques may be written in terms of their various components as follows (see Pasol, Sellier, & Feuillebois, 2010):

- For translation:

$$\mathbf{F}^{\mathrm{t}} = -6\pi a\mu\,[f^{\mathrm{t}}_{xx}(U_x\mathbf{i} + U_y\mathbf{j}) + f^{\mathrm{t}}_{zz}U_z\mathbf{k}], \tag{11a}$$

$$\mathbf{C}^{\mathrm{t}} = 8\pi a^2\mu c^{\mathrm{t}}_{yx}(U_x\mathbf{j} - U_y\mathbf{i}). \tag{11b}$$

- For rotation:

$$\mathbf{F}^{\mathrm{r}} = 6\pi a^2\mu f^{\mathrm{r}}_{xy}(\Omega_y\mathbf{i} - \Omega_x\mathbf{j}), \tag{12a}$$

$$\mathbf{C}^{\mathrm{r}} = -8\pi a^3\mu[c^{\mathrm{r}}_{yy}(\Omega_x\mathbf{i} + \Omega_y\mathbf{j}) + c^{\mathrm{r}}_{zz}\Omega_z\mathbf{k}]. \tag{12b}$$

- For the sphere held fixed in the linear shear flow $k_s z\mathbf{i}$:

$$\mathbf{F}^{\mathrm{s}} = 6\pi a\mu f^{\mathrm{s}}_{xx}k_{\mathrm{s}}\ell\,\mathbf{i}, \tag{13a}$$

$$\mathbf{C}^{\mathrm{s}} = 4\pi a^3\mu c^{\mathrm{s}}_{yx}k_{\mathrm{s}}\,\mathbf{j}. \tag{13b}$$

- For the sphere held fixed in the quadratic shear flow $k_{\mathrm{q}}z^2\mathbf{i}$:

$$\mathbf{F}^{\mathrm{q}} = 6\pi a\mu f^{\mathrm{q}}_{xx}k_{\mathrm{q}}\ell^2\,\mathbf{i}, \tag{14a}$$

$$\mathbf{C}^{\mathrm{q}} = 8\pi a^3\mu c^{\mathrm{q}}_{yx}k_{\mathrm{q}}\ell\,\mathbf{j}. \tag{14b}$$

These equations define dimensionless aerodynamic friction factors, denoted f for the forces and c for the torques. In (11)–(14), the first subscript of f and c shows the direction of the force and torque, respectively, and the second subscript stands for the direction of the translation or rotation velocity of the particle or the direction of the ambient flow. Note that these friction coefficients are components of friction tensors for more general flow fields. When considering the directions x and y parallel to the wall, various symmetry relationships have been applied in the above equations. The coefficients in (11)–(14) are chosen so that the friction factors $f^{\mathrm{t}}_{xx}, c^{\mathrm{r}}_{yy}, f^{\mathrm{s}}_{xx}, c^{\mathrm{s}}_{yx}, f^{\mathrm{q}}_{xx}, c^{\mathrm{q}}_{yx}$ have the limit of unity when the particle is far from the wall, $\ell/a \to \infty$. The coupling friction factors $c^{\mathrm{t}}_{yx}, f^{\mathrm{r}}_{xy}$ vanish for $\ell/a \to \infty$. Moreover, Lorentz reciprocal theorem (see e.g. Happel & Brenner, 1973) provides the relationship

$$f^{\mathrm{r}}_{xy} = \frac{4}{3}c^{\mathrm{t}}_{yx}.$$

When the particle is in contact with a rough wall, as recalled in the introduction, the effective aerodynamic influence of the wall is equivalent to a smooth plane wall located below the tip of corrugations, that is our *base plane*. The gap between this plane and the particle surface, expressed by

$$a\varepsilon = \ell - a,$$

is of the order of the average roughness. This roughness is assumed to be small compared with the particle, thus

$$\varepsilon \ll 1.$$

The classical theory of lubrication uses the assumption of a small gap between a body and a wall to obtain approximate solutions of the Stokes equations for the fluid motion between the body and the wall. Using the body scale a and the gap scale $a\varepsilon$ in the equations and expanding at first order in $\varepsilon \ll 1$ provide after some manipulation an equation for the pressure in the gap, the so-called "Reynolds equation". This equation may be solved analytically for a number of usual problems. Variations in pressure are high in the gap since the motion of the viscous fluid needs high pressure gradients in small apertures. Thus the force on the body is at first order obtained by integrating only the pressure on the body surface (that is, ignoring the viscous stresses).

The most classical result, attributed to G.I. Taylor (as presented by Hardy & Bircumshaw, 1925), is the expression for the drag coefficient on a spherical particle moving normal to a wall, $f^{\mathrm{t}}_{zz} \simeq 1/\varepsilon$. The pressure is so high when the gap decreases that it diverges when the gap vanishes. As a consequence the drag force diverges as well. This may be considered as a paradox from the Stokes equations for a viscous fluid.

For tangential motions, the resolution of the flow field is more complicated since the "inner" Reynolds equation at scale $a\varepsilon$ has to be supplemented by matching with an "outer" flow equation at scale a, see e.g. O'Neill and Stewartson (1967). Then the drag force contains singular terms in $\log \varepsilon$.

Various results for the friction factors of aerodynamic forces and torques have been obtained by various authors, see e.g. the review by Feuillebois (1989) for results and references. Considering the first orders in ε,

$$f^{\mathrm{t}}_{xx} \simeq -\frac{8}{15}\log\varepsilon + 0.9543 \tag{15a}$$

$$f^{\mathrm{t}}_{zz} \simeq \frac{1}{\varepsilon} - \frac{1}{5}\log\varepsilon + 0.9713 \tag{15b}$$

$$c^{\mathrm{t}}_{yx} \simeq -\frac{1}{10}\log\varepsilon - 0.1929 \tag{15c}$$

$$c^{\mathrm{r}}_{yy} \simeq -\frac{2}{5}\log\varepsilon + 0.3817 \tag{15d}$$

$$c^{\mathrm{r}}_{zz} \simeq 1.2020 \tag{15e}$$

$$f^{\mathrm{s}}_{xx} \simeq 1.7009 \tag{15f}$$

$$c^{\mathrm{s}}_{yx} \simeq 0.9440 \tag{15g}$$

$$f^{\mathrm{q}}_{xx} \simeq 1.9430 \tag{15h}$$

$$c^{\mathrm{q}}_{yx} \simeq 0.991 \tag{15i}$$

The singular terms in ε and $\log\varepsilon$ arise when surfaces are in relative motion. Indeed, note that no such terms arise in $c^{\mathrm{r}}_{zz}, f^{\mathrm{s}}_{xx}, c^{\mathrm{s}}_{yx}, f^{\mathrm{q}}_{xx}, c^{\mathrm{q}}_{yx}$, since the particle is then fixed relative to the wall in an ambient flow field.

As for the singular friction factors, the paradox of a force or torque becoming infinite at $\varepsilon \to 0$ disappears when considering various physical phenomena: the elasticity of surfaces (Davis, Serayssol, & Hinch, 1986), a slip boundary condition on surfaces at small scales, possibly combined with elasticity effects (Vinogradova & Feuillebois, 2000), the roughness of surfaces (Ekiel-Jeżewska et al., 1999, 2002). This last case is considered here: the friction factors do not diverge when considering a rough wall since ε is always strictly positive.

Simple lubrication expressions in (15) are useful since they allow us to obtain simple analytical results for various problems when the gap is small. Now, when the particle is located at any distance from the wall, the full Stokes equations of fluid motion have to be solved. Using the appropriate technique of bispherical coordinates, Chaoui & Feuillebois (2003) and Pasol, Sellier, & Feuillebois, (2006) calculated accurate values of the friction factors which will also be used in calculations of particle trajectories presented below.

3.3. Adhesion force

The force necessary to pull off a spherical particle from a smooth surface depend on the surface energy $\mathcal{E}_A$. Classical models of adhesion forces are those of Johnson, Kendall and Roberts (JKR) giving

$$F_{\mathrm{JKR}} = \frac{3}{2}\pi a \mathcal{E}_A$$

and Derjaguin, Müller and Toporov (DMT) giving

$$F_{\mathrm{DMT}} = 2\pi a \mathcal{E}_A.$$

For instance from Valega-Mackenzie & Thijsse (2013) the energy of adhesion of alumina onto epoxy is around $\mathcal{E}_A = 0.7\,\mathrm{J/m^2}$. For a particle with diameter $2a = 10\,\mu\mathrm{m}$, $F_{\mathrm{JKR}} = 16\,\mu\mathrm{N}$ and $F_{\mathrm{DMT}} = 22\,\mu\mathrm{N}$. For smooth surfaces, actual values depend on physical elasticity parameters of the surfaces and are intermediate between those results.

In the JKR model, the contact radius of the deformed elastic sphere is, when at separation:

$$r_c = \left(\frac{4aF_{\mathrm{JKR}}}{K}\right)^{1/3}, \tag{16}$$

where

$$K=\frac{4}{3}\left(\frac{1-\nu_1^2}{E_1}+\frac{1-\nu_2^2}{E_2}\right)^{-1}$$

is the equivalent Young modulus. Here, E_1 and E_2 are the Young moduli of the materials 1 and 2, respectively and ν_1,ν_2 are their Poisson coefficients. For example, using index 1 for alumina and 2 for epoxy,

$$E_1=390\text{ GPa},\quad \nu_1=0.27,\quad E_2=3.5\text{ GPa},\quad \nu_2=0.4,$$

giving $K=5.5$ GPa and $r_c=250$ nm.

More importantly, adhesion depends on surface roughness. Models by Soltani & Ahmadi (1995) and Soltani, Ahmadi, Bayer, & Gaynes (1995), as summarized by Zhang, Ahmadi, Qian, & Ferro (2008), show that the adhesion force for rough surfaces is very small compared with F_{DMT}. The contact radius r_c is also smaller than (16). Note also that Peressadko, Hosoda, & Persson (2005) show that when the standard deviation of roughness increases from 0.04 to 0.2 μm, the effective surface energy decays from $\mathcal{E}_A$ to practically zero (the variation of this energy is displayed in their Fig. 3). Cheng, Dunn, & Brach (2002) similarly obtain an asymptotic decay to zero of the adhesion force (see their Fig. 17).

For AFM experiments that we conducted with a 5 μm alumina particle on a rough epoxy substrate, the average roughness was around 20–40 nm, with some isolated large peaks (>200 nm). The adhesion force was found in the range of 1–40 nN, with a median of 18 nN. Details are provided in Appendix A. Using this value of the adhesion force in JKR formula (16) gives the estimate $r_c=20$ nm. We will use these data of adhesion forces as typical values in the calculations of a particle in contact with a rough wall of average roughness around 30 nm. For the calculations, we will also consider larger particles (20 and 40 μm) with the same wall roughness. Since there are no data for the adhesion force, we will take estimates in the range 20–40 nN.

4. Motion of a particle in contact with a rough wall

We assume here that the ambient flow field is strong enough for the particle to start moving along the rough wall, while staying in contact with it in a circular region of center H at $\mathbf{x}_H$ and radius r_c. Let $\mathbf{H}=H_x\mathbf{i}+H_z\mathbf{k}$ be the reaction force of the wall onto the particle.

4.1. Equations of motion

The condition for the particle to start will be made precise below in Section 4.2. Because of the random roughness, the particle when pushed by the fluid in the x direction may also wander in the y direction along the wall. However, we assume that on average, the displacement in the y direction vanishes (note that it may not be the case for a roughness designed as stripes at an angle to the flow direction).

Also, the event of a particle stopping during its rolling motion, probably due to a locally smoother surface and therefore to a higher adhesion force, will not be considered here. Indeed, it is not relevant in the focus of the present paper, that is the encounter of a rolling particle with a high peak of roughness, see Sections 5 and following ones.

The translational velocity in the x direction and rotational velocity in the y direction of the particle are obtained from the particle equations of motion:

$$m\frac{\mathrm{d}U_x}{\mathrm{d}t}=F_x+H_x \tag{17a}$$

$$0=-W+H_z \tag{17b}$$

$$I\frac{\mathrm{d}\Omega_y}{\mathrm{d}t}=C_y-\ell H_x-r_cH_z, \tag{17c}$$

where I is the moment of inertia of the particle. Assuming the particle to be homogeneous, $I=\frac{2}{5}ma^2$. In (17c), we have considered that when the particle is moving the reaction torque results from the reaction force applied at the edge r_c of the contact region. As for the value of ℓ in (17c), note that:

(i) since the contact region is small, the thickness (in the z direction) of the flattened part of the particle may be neglected with a second order error in r_c/a;
(ii) thus, since the roughness is small, the moment of force H_x may be approximated by $\ell H_x\simeq aH_x$.

From (17b), the normal component of the reaction force is simply

$$H_z=W. \tag{18}$$

The value of the component H_x depends on the motion of the contact region.

4.2. Condition for particle to start

The particle is starting whenever $\frac{dU_x}{dt} \geq 0$ and $\frac{d\Omega_y}{dt} \geq 0$. From (17a)–(17c) and the above assumptions, eliminating H_x gives the necessary condition:

$$F_x + \frac{C_y}{a} \geq \frac{r_c}{a} W \tag{19}$$

Using the expressions (10) with (13)–(14) of the aerodynamic force and torque on a particle at rest and using again $\ell \simeq a$, the condition is:

$$f^s_{xx} + f^q_{xx} \widetilde{k}_q + \frac{2}{3} c^s_{yx} + \frac{4}{3} c^q_{yx} \widetilde{k}_q \geq \widetilde{r}_c \widetilde{V}_s \tag{20}$$

in which $\widetilde{r}_c = r_c/a$ and $\widetilde{V}_s = V_s/(ak_s)$ with V_s defined in (6). Using the values (15) of the friction factors when in lubrication, the condition (20) gives:

$$2.330 + 3.264 \widetilde{k}_q \geq \widetilde{r}_c \widetilde{V}_s. \tag{21}$$

4.3. Rolling without slip

If the particle rolls on the wall without slipping,

$$U_x = \Omega_y a. \tag{22}$$

Solving the linear system (17a), (17c) with (22), for the unknowns $m\, dU_x/dt$ and H_x, we obtain:

$$m\frac{dU_x}{dt} = \frac{5}{7}\left(F_x + \frac{C_y}{a} - \frac{r_c}{a} W\right), \tag{23}$$

$$H_x = -\frac{2}{7} F_x + \frac{5}{7}\frac{C_y}{a} - \frac{5}{7}\frac{r_c}{a} W. \tag{24}$$

This regime of rolling without slip is possible only provided that the static friction force H_x stays within the limits of Amonton–Coulomb's law of solid friction, that is:

$$|H_x| \leq \mu_s H_z, \tag{25}$$

where μ_s is the static friction coefficient. This coefficient depends on the materials and structure of the surfaces. A standard value of 0.2 will be used in calculations below.

Consider a steady rolling motion, $m\, dU_x/dt = 0$. Using the expressions (10) with (11)–(14) of the aerodynamic force and torque together with the values (15) of the friction factors when in lubrication, the normalized translation velocity $\widetilde{U}_x = U_x/(ak_s)$ is found to be:

$$\widetilde{U}_x = \frac{2.330 + 3.264\, \widetilde{k}_q - \widetilde{r}_c \widetilde{V}_s}{0.800 \log \frac{1}{\varepsilon} + 1.978}, \tag{26}$$

The solid friction (24) at the wall is then found to be:

$$H_x = -\mu a^2 k_s \left(10.10 + 5.858\, \widetilde{k}_q + 9.429\, \widetilde{r}_c \widetilde{V}_s\right). \tag{27}$$

From these results, the limit of static friction (25) may be written in dimensionless form as:

$$0.5359 + 0.3109\, \widetilde{k}_q \leq (\mu_s - 0.5\, \widetilde{r}_c) \widetilde{V}_s. \tag{28}$$

Numerical values of r_c for particles with low elasticity, as considered in Section 3.3, show that $\widetilde{r}_c \ll \mu_s$. Thus the contact radius has little influence on the rolling without slip limit for such particles.

Consider a 10 μm diameter particle with a 30 nm wall roughness and a linear shear flow with shear rate $k_s = 10^5\ s^{-1}$. Using $\mu = 1.8 \times 10^{-5}$ Pa · s for air, we find $\widetilde{V}_s \simeq 18$. Then the particle rolls without slip with translation velocity as given from Eq. (26): $\widetilde{U}_x \simeq 0.39$. That is, the particle center velocity is 0.39 times the ambient air velocity at its distance from the wall.

4.4. Rolling with slip

Whenever Amonton–Coulomb's condition (25) is not satisfied, there is rolling with slip. Then, the solid friction force along the wall is

$$|H_x| = \mu_d H_z, \tag{29}$$

where μ_d is the dynamic friction coefficient, the value of which is usually less than μ_s (typical values taken below in the

calculations are $\mu_s = 0.2$ and $\mu_d = 0.1$). The result (18) then gives:

$$|H_x| = \mu_d W.$$

The equations of motion (17a) and (17c) then provide the translation velocity U_x and rotation velocity Ω_y. Assuming the rolling motion to be steady, $\mathrm{d}U_x/\mathrm{d}t = \mathrm{d}\Omega_y/\mathrm{d}t = 0$, and using again (10), (11)–(14), with the lubrication friction factors (15), the normalized translation velocity $\widetilde{U}_x = U_x/(ak_s)$ and rotation velocity $\widetilde{\Omega}_y = \Omega_y/k_s$ are found to be:

$$\widetilde{U}_x = \Big[\Big(0.7433 + 0.9093\widetilde{k}_q - (0.3\mu_d + 0.1\widetilde{r}_c)\widetilde{V}_s\Big)\log(1/\varepsilon) + 0.5278 + 0.4868\widetilde{k}_q - (0.5746\mu_d - 0.1929\widetilde{r}_c)\widetilde{V}_s\Big] \Big/ \Big[0.2(\log(1/\varepsilon))^2 + 0.6367\log(1/\varepsilon) + 0.3146\Big] \tag{30a}$$

$$\widetilde{U}_x \simeq \frac{1}{\log\dfrac{1}{\varepsilon}}\Big[3.7165 + 4.5467\,\widetilde{k}_q - (1.5\mu_d + 0.5\widetilde{r}_c)\widetilde{V}_s\Big] \tag{30b}$$

$$\widetilde{\Omega}_y = \Big[\Big(0.4218 + 0.7228\widetilde{k}_q + (0.3\mu_d - 0.4\widetilde{r}_c)\widetilde{V}_s\Big)\log(1/\varepsilon) + 0.1223 + 0.5709\widetilde{k}_q + (0.9086\mu_d - 0.7157\widetilde{r}_c)\widetilde{V}_s\Big] \Big/ \Big[0.2(\log(1/\varepsilon))^2 + 0.6367\log(1/\varepsilon) + 0.3146\Big] \tag{30c}$$

$$\widetilde{\Omega}_y \simeq \frac{1}{\log\dfrac{1}{\varepsilon}}\Big[2.1091 + 3.6142\,\widetilde{k}_q + (1.5\mu_d - 2\widetilde{r}_c)\widetilde{V}_s\Big]. \tag{30d}$$

The results (30b) and (30d) are the first order approximations in ε of (30a) and (30c), respectively.

Since usually $\widetilde{r}_c \ll \mu_d$ (typically $\widetilde{r}_c = 0.008$ for a 5 μm diameter particle, see Section 3.3, and $\mu_d \simeq 0.1$), the radius of contact has little influence on the rolling with slip motion.

Note that in the particular case of a perfect slip $\mu_d = 0$ and a pure linear shear flow ($k_q = 0$), the results (30b) and (30d) give in the limit $\varepsilon \to 0$ the asymptotic result:

$$\frac{\widetilde{\Omega}_y}{\widetilde{U}_x} = \frac{a\Omega_y}{U_x} = 0.5675.$$

That is, the rotation velocity is about half of that for rolling without slip. This result was already obtained by Goldman et al. (1967). In the case of a partial slip, as considered here, the asymptotic result gives $\widetilde{\Omega}_y/\widetilde{U}_x > 0.5675$. For instance, using the same physical values as in Section 4.3, we find that a particle with diameter $d = 50$ μm slips while rolling with velocities $\widetilde{U}_x = 0.55, \widetilde{\Omega}_y = 0.29$, so that $\widetilde{\Omega}_y/\widetilde{U}_x = 0.57$.

5. Particle in contact with a rough wall and a large peak of roughness

5.1. Model

From the preceding sections, we can calculate the velocity of a particle being pushed steadily by an airflow along a rough wall. At some stage, the particle will encounter a peak that is higher than the average roughness.

The case in which the particle bounces on the peak is not the focus of the paper. It is discussed in Appendix B. Whether the collision is elastic is not obvious since plastic deformation may occur between the peak and the particle. Provided that the collision is sufficiently elastic and that the particle kinetic energy after bouncing overcomes its adhesion energy to the wall, the particle may move freely up. Integrating the momentum equation for the inertial vertical motion provides the maximum vertical position that the particle may reach before falling down because of its weight. The detailed problem of elastic or non-elastic collision is left for future study. We assume below that particle does not bounce on the peak but rather stays attached to it.

The equations of motion of a particle in contact with both a rough wall and a peak are considered in this section. We are concerned in the possibility of onset of lifting of the particle by the air flow in a rotating motion about the peak. Since both components of the friction reaction force along the wall produce a torque about the peak, their contribution has to be discussed in detail.

Let us first introduce the coordinates system and notation appropriate to the peak and moving particle, then discuss the presence of isolated peaks based on experimental evidence, and finally write the equations of motion of the particle.

5.2. Coordinates system and notation

The notation is presented in Fig. 1, see also two-dimensional views in Fig. 3. In the (x, y, z) Cartesian system of coordinates, let the origin $x = 0$ be defined as the abscissa of the sphere center in the $y = 0$ plane when the sphere in contact with the rough wall comes for the first time in contact with the peak P. Let O_0 be the position of the sphere center at this time. The large peak of roughness is modeled as a material line segment whose end point P is located at some distance δ from the

base plane wall, with coordinates $\mathbf{x}_P = (\beta, 0, \delta)$. The value of δ is larger than the average roughness, yet small compared with a. Let P' be the projection of P onto the $z=0$ plane.

Let us define a Cartesian coordinates system (x_1, x_2, x_3) that is at rest in the (x, y, z) frame. Let its origin coincide with the projection H' of the sphere center O onto the base plane at the considered time. Let the x_1-axis be along $H'P'$ and the x_3-axis along $H'O$, so that $x_3 = z$. Let $(\mathbf{e}_1, \mathbf{e}_2, \mathbf{e}_3)$ be the orthonormal base of the (x_1, x_2, x_3) frame, with values:

$$\mathbf{e}_1 = \frac{\mathbf{n} - (\mathbf{n}\cdot\mathbf{k})\mathbf{k}}{|\mathbf{n} - (\mathbf{n}\cdot\mathbf{k})\mathbf{k}|} \tag{31a}$$

$$\mathbf{e}_2 = \mathbf{k}\wedge\mathbf{e}_1 = \frac{\mathbf{k}\wedge\mathbf{n}}{|\mathbf{n} - (\mathbf{n}\cdot\mathbf{k})\mathbf{k}|} \tag{31b}$$

$$\mathbf{e}_3 = \mathbf{k}. \tag{31c}$$

Note that (31a) may be also written as:

$$\mathbf{n} = n_1\mathbf{e}_1 + n_3\mathbf{e}_3, \quad \text{with } n_1 = |\mathbf{n} - (\mathbf{n}\cdot\mathbf{k})\mathbf{k}|, \quad n_3 = \mathbf{n}\cdot\mathbf{k}. \tag{32}$$

In the (x_1, x_2, x_3) frame, the particle moves with a translation velocity

$$\mathbf{U} = U_1\mathbf{e}_1 + U_2\mathbf{e}_2 + U_3\mathbf{e}_3$$

and a rotation velocity

$$\boldsymbol{\Omega} = \Omega_1\mathbf{e}_1 + \Omega_2\mathbf{e}_2 + \Omega_3\mathbf{e}_3.$$

Since the sphere is in contact with the plane and the peak, $U_1 = U_3 = 0$. The only leftover component of $\mathbf{U}$ is U_2.

Let

$$\mathbf{P} = P_1\mathbf{e}_1 + P_2\mathbf{e}_2 + P_3\mathbf{e}_3$$

be the reaction force of the peak onto the sphere at point P. We assume that the sphere rolls around point P without slipping, that is the peak stays always in contact with the same point of the sphere surface. Thus the sphere velocity at P is zero. This may be written with the definition of $\mathbf{n}$:

$$\mathbf{U} + \boldsymbol{\Omega}\wedge\mathbf{n}a = 0 \tag{33}$$

Since $\mathbf{U} = U_2\,\mathbf{e}_2$, (33) gives $\Omega_2 = 0$.

Two cases may be considered below, rolling without and with slip on the wall.

5.3. Experimental evidence of isolated peaks

From the experimental data presented in Appendix A, the roughness appears for typical surfaces as an average background plus isolated peaks. A zoom on Fig. A1 (left-hand-side, in which the scale saturates at the height of 200 nm) is shown

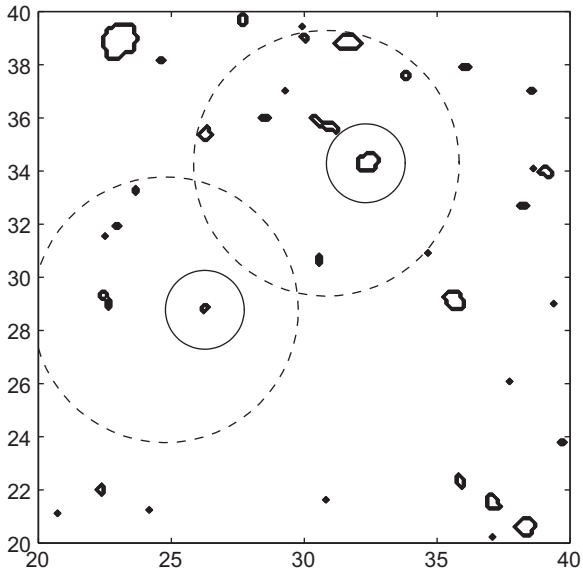

Fig. 2. Part of Fig. A1, left (dimensions in micrometers). The contours of the highest peaks (larger than 200 nm and appearing as white spots in Fig. A1) have been extracted. For two typical peaks P assumed to be of height 200 nm and for a 10 μm diameter particle, the circle of center P' and radius $P'H'$ (see Fig. 1) is drawn as a solid line. The size of the particle itself is represented as a dashed circle for comparison.

in Fig. 2. Consider a typical particle of diameter $2a = 10\ \mu$m in diameter in contact with a peak of height $\delta = 200$ nm. A solid circle in the figure presents possible positions of the projection H' of the sphere center around a peak. The circle is centered at the peak and its radius is $P'H'$, the value of which is of order $\sqrt{2a\delta}$ (since $\delta \ll a$). The size of the particle itself is represented as a dashed circle for comparison.

It appears that a particle (10 μm in diameter as a typical one) is generally not in contact with more than one peak, when it is a contact with the rough wall. Indeed, the solid circles shown in Fig. 2 in general *do not contain* another peak (only two circles are represented but this appears fairly general). Thus, there is a significant experimental presence of isolated peaks for the surfaces considered here. This result will be the basis for our model which will consider the encounter of a particle with a single peak.

Now in the same figure, there are a few cases for which a particle may be in contact with two high peaks. Also, for surfaces with a higher density of peaks as compared with the particle size, a particle might in general be in contact with two peaks. This is the case generally considered by the "Rock n' Roll" model introduced by Reeks & Hall (2001). However, to our knowledge, that model is limited to a 2-D configuration in which the peaks are aligned with the ambient flow field. The 3-D configuration of a particle in contact with two peaks which are *not* aligned with the ambient flow field would deserve a special treatment that would be analogous to the one presented here for one peak.

5.4. Equations of motion for rolling without slip around a peak

When the particle rolls without slip along the rough wall, the contact region distorts and follows a caterpillar track while being displaced along the sphere surface. However, at the scale of the sphere radius, this displacement is very small compared with that of the sphere center and can be neglected. Thus, we assume that the sphere velocity at the center H of the contact region vanishes during the rolling motion:

$$\mathbf{U} - \boldsymbol{\Omega} \wedge \mathbf{k}a = 0. \tag{34}$$

Subtracting (34) from (33) gives

$$(\mathbf{k} + \mathbf{n}) \wedge \boldsymbol{\Omega} = 0. \tag{35}$$

Thus, $\boldsymbol{\Omega}$ is parallel to $\mathbf{k}+\mathbf{n}$. Since point P is fixed, the sphere rotates around the line HP. Solving the system (33)–(34) gives:

$$\Omega_1 = -\frac{U_2}{a}, \tag{36}$$

$$\Omega_3 = -\frac{U_2(1+n_3)}{an_1}. \tag{37}$$

The equations of motion of the particle are

$$m\frac{\mathrm{d}\mathbf{U}}{\mathrm{d}t} = \mathbf{W} + \mathbf{F} + \mathbf{P} + \mathbf{H}, \tag{38}$$

$$I\frac{\mathrm{d}\boldsymbol{\Omega}}{\mathrm{d}t} = \mathbf{C} + (\mathbf{x}_P - \mathbf{x}_O) \wedge \mathbf{P} + (\mathbf{x}_H - \mathbf{x}_O) \wedge \mathbf{H}. \tag{39}$$

Let (H_1, H_2, H_3) be the components of the reaction force $\mathbf{H}$ of the wall at point H. Taking into account the preceding expressions for the velocities and forces, let us project (38)–(39) onto the base vectors $(\mathbf{e}_1, \mathbf{e}_2, \mathbf{e}_3)$, Eqs. (31):

$$0 = F_1 + P_1 + H_1 \tag{40a}$$

$$m\frac{\mathrm{d}U_2}{\mathrm{d}t} = F_2 + P_2 + H_2 \tag{40b}$$

$$0 = -W + P_3 + H_3 \tag{40c}$$

$$-\frac{2}{5}m\frac{\mathrm{d}U_2}{\mathrm{d}t} = \frac{C_1}{a} - n_3P_2 + H_2 \tag{41a}$$

$$0 = \frac{C_2}{a} + n_3P_1 - n_1P_3 - H_1 \tag{41b}$$

$$-\frac{2}{5}\frac{n_3+1}{n_1}m\frac{\mathrm{d}U_2}{\mathrm{d}t} = \frac{C_3}{a} + n_1P_2. \tag{41c}$$

These equations for rolling without slip are valid provided the reaction force $H_3 > 0$ from the plane and the reaction force H_1 satisfy the limits of Amonton–Coulomb's law of solid friction:

$$|H_1| < \mu_s H_3. \tag{42}$$

5.5. Escaping an undetermined problem

The equations of motion (40)–(41) provide a linear system of six equations to be solved for the seven unknowns $(m\,\mathrm{d}U_2/\mathrm{d}t, P_1, P_2, P_3, H_1, H_2, H_3)$. Thus, the system is undetermined. This is more easily understood by noting that in order to determine the four reaction forces (P_1, P_3, H_1, H_3) which are responsible for the balance in the (x_1, x_3) plane, there are only three equations (40a), (40c), (41b). This problem is hyperstatic. Indeed, there is a geometrical constraint between points H and P which may be either considered on the side of the sphere or on the side of the obstacle P attached to the wall. It is thus clear that to this geometrical constraint of equal distances may be associated an unknown force.

In classical hyperstatic problems, some more physical properties, like elastic ones, should be added to resolve the indeterminacy. Here, we will simply take the tangential force H_1 as a parameter and then from the results discuss the constraints to be applied to H_1.

The solution of the linear system (40)–(41) as a function of H_1 is:

$$m\frac{\mathrm{d}U_2}{\mathrm{d}t} = -\frac{5n_1^2}{(1+n_3)(5n_3-9)}\left(F_2-\frac{C_1}{a}\right)+\frac{5n_1}{5n_3-9}\frac{C_3}{a} \tag{43a}$$

$$P_1 = -F_1 - H_1 \tag{43b}$$

$$P_2 = \frac{2}{5n_3-9}\left(F_2-\frac{C_1}{a}\right)+\frac{7n_1}{(1+n_3)(5n_3-9)}\frac{C_3}{a} \tag{43c}$$

$$P_3 = -\frac{n_3}{n_1}F_1+\frac{C_2}{an_1}-\frac{n_3+1}{n_1}H_1 \tag{43d}$$

$$H_2 = \frac{2}{5n_3-9}F_2-\frac{5n_3-7}{5n_3-9}\frac{C_1}{a}+\frac{n_1(5n_3-2)}{(1+n_3)(5n_3-9)}\frac{C_3}{a} \tag{43e}$$

$$H_3 = \frac{n_3}{n_1}F_1-\frac{C_2}{an_1}+W+\frac{n_3+1}{n_1}H_1. \tag{43f}$$

The focus here is about the possibility of the sphere to be lifted from the wall by the airflow. This happens whenever the H_3 reaction force vanishes. Because of Amonton–Coulomb's law (42), then the reaction force H_1 should vanish at the same time. From (43f), we are left with the condition:

$$C_2 - an_3F_1 = an_1W. \tag{44}$$

Let us define the angle $\Phi = \widehat{HOP}$ (see Fig. 1). Then,

$$n_3 = -\cos\,\Phi, \quad n_1 = \sin\,\Phi. \tag{45}$$

The lifting condition (44) is also written:

$$C_2 + a\,\cos\,\Phi\,F_1 = a\,\sin\,\Phi\,W. \tag{46}$$

The locations of point P that are the most favourable for the particle to be lifted around it are for small Φ. This will be studied in more detail below by introducing the aerodynamic force and torque.

5.6. Equations of motion for rolling with slip around a peak

Whenever (42) is not satisfied, the particle rolls with slip on the plane. Again here, since the sphere is in contact with the plane and the peak, $U_1 = U_3 = 0$ and the only non-zero component is U_2. Moreover with (33), we have

$$\Omega_2 = 0, \tag{47}$$

$$\Omega_3 = -\frac{U_2 - \Omega_1 an_3}{an_1}. \tag{48}$$

Consider without lack of generality the case $U_2 > 0$. The friction force in this direction, H_2, is related to the normal reaction component H_3 by the dynamic friction condition:

$$H_2 = -\mu_d H_3. \tag{49}$$

Projecting the equations of motion (38)–(39) onto the axes (x_1, x_2, x_3) then gives:

$$0 = F_1 + P_1 + H_1 \tag{50a}$$

$$m\frac{\mathrm{d}U_2}{\mathrm{d}t} = F_2 + P_2 + H_2 \tag{50b}$$

$$0 = -W + P_3 + H_3, \tag{50c}$$

$$\frac{2}{5}ma\frac{d\Omega_1}{dt}=\frac{C_1}{a}-n_3P_2+H_2 \tag{51a}$$

$$0=\frac{C_2}{a}+n_3P_1-n_1P_3-H_1 \tag{51b}$$

$$\frac{2n_3}{5n_1}ma\frac{d\Omega_1}{dt}-\frac{2}{5n_1}m\frac{dU_2}{dt}=\frac{C_3}{a}+n_1P_2. \tag{51c}$$

This is linear system of 7 equations (49)–(51) for 8 unknowns

$$\left(m\frac{dU_2}{dt}, ma\frac{d\Omega_1}{dt}, P_1, P_2, P_3, H_1, H_2, H_3\right),$$

thus the problem is also undetermined in this case.

5.7. Assuming slip in both directions on wall

Like for the rolling without slip, the system seems here to be hyperstatic in the (x_1, x_3) plane. However, if the particle slips in the x_2 direction, there is a relative motion of surfaces. Consequently, it also slips in the perpendicular direction x_1. This physical remarks leads us to conclude that system cannot be hyperstatic. Thus we propose to use for H_1 a dynamic slip condition like (49), that is:

$$H_1=-\mu_d H_3 \tag{52}$$

Solving then the linear system of 8 equations (49)–(52), we obtain:

$$m\frac{dU_2}{dt}=\frac{5}{7}F_2+\frac{5n_3}{7}\frac{C_1}{a}+\frac{5}{7}\frac{\mu_d(n_3+1)}{(n_1+\mu_d(n_3+1))}\left[-n_3F_1+\frac{C_2}{a}-n_1W\right]-\frac{5}{7}\frac{(1+n_3)(-n_3+1+\mu_d n_1)}{(n_1+\mu_d(n_3+1))}\frac{C_3}{a} \tag{53a}$$

$$ma\frac{d\Omega_1}{dt}=\frac{5n_3}{7}F_2-\frac{5(-7+5n_3^2)}{14}\frac{C_1}{a}-\frac{5}{14}\frac{\mu_d(n_3+1)(5n_3-7)}{(n_1+\mu_d(n_3+1))}\left[-n_3F_1+\frac{C_2}{a}-n_1W\right]+\frac{25}{14}\frac{n_3(1+n_3)(-n_3+1+\mu_d n_1)}{(n_1+\mu_d(n_3+1))}\frac{C_3}{a} \tag{53b}$$

$$P_1=\frac{-(n_1+\mu_d)F_1-\mu_d C_2/a+n_1\mu_d W}{(n_1+\mu_d(n_3+1))} \tag{53c}$$

$$P_2=-\frac{2}{7}F_2+\frac{5n_3}{7}\frac{C_1}{a}+\frac{1}{7}\frac{\mu_d(-2+5n_3)}{(n_1+\mu_d(n_3+1))}\left[-n_3F_1+\frac{C_2}{a}-n_1W\right]-\frac{5}{7}\frac{(1+n_3)(-n_3+1+\mu_d n_1)}{(n_1+\mu_d(n_3+1))}\frac{C_3}{a} \tag{53d}$$

$$P_3=\frac{1}{(n_1+\mu_d(n_3+1))}\left[-n_3F_1+\frac{C_2}{a}+\mu_d(n_3+1)W\right] \tag{53e}$$

$$H_1=-\mu_d H_3 \tag{53f}$$

$$H_2=-\mu_d H_3 \tag{53g}$$

$$H_3=\frac{1}{(n_1+\mu_d(n_3+1))}\left[n_3F_1-\frac{C_2}{a}+n_1W\right]. \tag{53h}$$

The sphere may be lifted whenever H_3 vanishes. We then obtain the same condition as in the case of rolling without slip, that is (44) (also written as (46)).

6. Motion of the lifted particle

6.1. Equations of motion for the particle attached to the peak

When the particle is lifted from the wall, any condition of velocity in H as well as on U_3 has to be dropped and the problem should be reconsidered. Note, however, that the particle is still in contact with wall at H at the beginning of the lifting motion when the force at this point vanishes. The sphere is assumed to stay in contact with the peak at point P during its whole motion, thus we should keep Eq. (33). We then have:

$$U_1=-an_3\Omega_2, \tag{54}$$

$$U_3=an_1\Omega_2, \tag{55}$$

$$\Omega_3=-\frac{U_2}{an_1}+\frac{n_3}{n_1}\Omega_1. \tag{56}$$

The equations of motion of the particle are:

$$m\frac{\mathrm{d}\mathbf{U}}{\mathrm{d}t}=\mathbf{W}+\mathbf{F}+\mathbf{P}, \tag{57a}$$

$$I\frac{\mathrm{d}\boldsymbol{\Omega}}{\mathrm{d}t}=\mathbf{C}+(\mathbf{x}_P-\mathbf{x}_O)\wedge\mathbf{P}, \tag{57b}$$

where $\mathbf{W}$ includes the adhesion force (when at contact) and the weight. Projecting them onto the base vectors $(\mathbf{e}_1,\mathbf{e}_2,\mathbf{e}_3)$ (see Eqs. (31)) gives:

$$-n_3 ma\frac{\mathrm{d}\Omega_2}{\mathrm{d}t}=F_1+P_1 \tag{58a}$$

$$m\frac{\mathrm{d}U_2}{\mathrm{d}t}=F_2+P_2 \tag{58b}$$

$$n_1 ma\frac{\mathrm{d}\Omega_2}{\mathrm{d}t}=-W+P_3 \tag{58c}$$

$$\frac{2}{5}ma\frac{\mathrm{d}\Omega_1}{\mathrm{d}t}=\frac{C_1}{a}-n_3P_2 \tag{59a}$$

$$\frac{2}{5}ma\frac{\mathrm{d}\Omega_2}{\mathrm{d}t}=\frac{C_2}{a}+n_3P_1-n_1P_3 \tag{59b}$$

$$-\frac{2}{5n_1}m\frac{\mathrm{d}U_2}{\mathrm{d}t}+\frac{2n_3}{5n_1}ma\frac{\mathrm{d}\Omega_1}{\mathrm{d}t}=\frac{C_3}{a}+n_1P_2. \tag{59c}$$

This is a linear system of six equations (58) and (59) for six unknowns

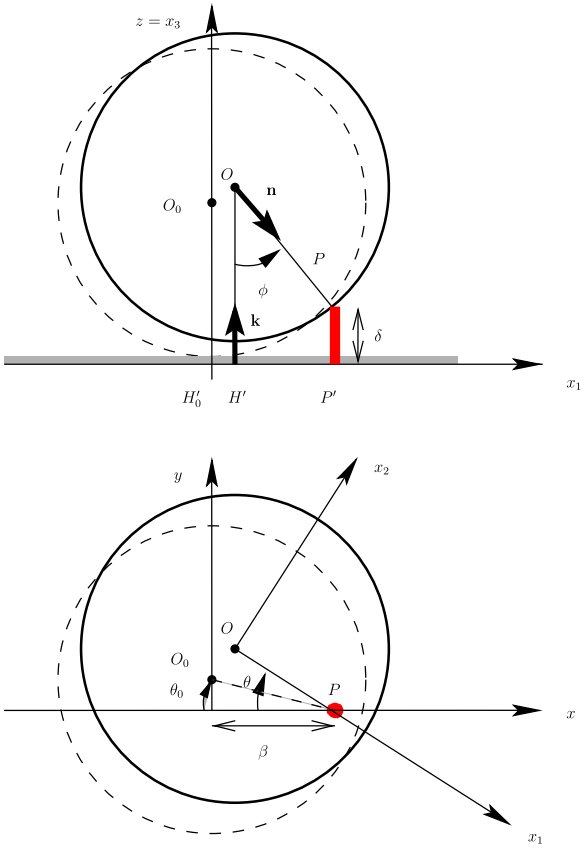

Fig. 3. Sketch of a spherical particle of radius a and center O being lifted at some time $t>0$ around a peak of roughness P; top: view from the side in the plane of O and P; bottom: view from the top. The solid circle represents the lifted particle at time $t>0$. The dashed circle represents the particle at time $t=0$ before being lifted: it is centered at point O_0 with coordinates $x=0, y=\beta\ \sin\ \theta_0, z=\ell'=a(1+\varepsilon)=\delta+a\ \cos\ \Phi$. The gray area in the top view represents the average roughness above the base plane $z=0$. The points H_0', H', P' are projections of O_0, O, P respectively onto the base plane.

$$\left(m\frac{\mathrm{d}U_2}{\mathrm{d}t}, ma\frac{\mathrm{d}\Omega_1}{\mathrm{d}t}, ma\frac{\mathrm{d}\Omega_2}{\mathrm{d}t}, P_1, P_2, P_3\right),$$

whose solution is:

$$m\frac{\mathrm{d}U_2}{\mathrm{d}t} = \frac{5}{7}F_2 + \frac{5}{7}n_3\frac{C_1}{a} - \frac{5}{7}n_1\frac{C_3}{a} \tag{60a}$$

$$ma\frac{\mathrm{d}\Omega_1}{\mathrm{d}t} = \frac{5}{7}n_3F_2 + \left(\frac{5}{2} - \frac{25}{14}n_3^2\right)\frac{C_1}{a} + \frac{25}{14}n_1n_3\frac{C_3}{a} \tag{60b}$$

$$ma\frac{\mathrm{d}\Omega_2}{\mathrm{d}t} = -\frac{5}{7}n_3F_1 + \frac{5}{7}n_1F_3 + \frac{5}{7}\frac{C_2}{a} - \frac{5}{7}n_1W \tag{60c}$$

$$P_1 = \left(-1 + \frac{5}{7}n_3^2\right)F_1 - \frac{5}{7}n_3\frac{C_2}{a} + \frac{5}{7}n_1n_3(W - F_3) \tag{60d}$$

$$P_2 = -\frac{2}{7}F_2 + \frac{5}{7}n_3\frac{C_1}{a} - \frac{5}{7}n_1\frac{C_3}{a} \tag{60e}$$

$$P_3 = -\frac{5}{7}n_1n_3F_1 + \frac{5}{7}n_1\frac{C_2}{a} + \left(\frac{2}{7} + \frac{5}{7}n_3^2\right)(W - F_3). \tag{60f}$$

The translation and rotation of the sphere are given by integrating equations (60a)–(60c) which depend only on the aerodynamic force **F** and torque **C** which are functions of the sphere translation and rotation velocity, see Section 3.2. Since the sphere escapes from the wall, we will not use the lubrication friction coefficients (15) but rather more general expressions of the friction coefficients derived from the accurate results obtained by Chaoui & Feuillebois (2003) and Pasol, Sellier, & Feuillebois, (2006) (these expressions contain lubrication as a particular case for small gaps).

6.2. *Lifted particle equations in terms of aerodynamic friction factors*

Let θ be the angle between the x and x_1 axes, see Figs. 1 and 3. Then,

$$\mathbf{e}_1 = \mathbf{i}\ \cos\ \theta - \mathbf{j}\ \sin\ \theta, \tag{61a}$$

$$\mathbf{e}_2 = \mathbf{i}\ \sin\ \theta + \mathbf{j}\ \cos\ \theta. \tag{61b}$$

When the particle comes in contact with the peak, say at time $t=0$, let $\theta = \theta_0$. The second relevant angle is that between vectors **OH** and **OP**, say ϕ. Then Φ is the value of ϕ when the particle is not lifted (in particular at $t=0$, but possibly also later on).

The coordinates of the sphere center O at time $t > 0$ then are

$$(a\ \sin\ \phi\ \cos\ \theta, a\ \sin\ \phi\ \sin\theta, \delta + a\ \cos\ \phi),$$

where $\phi = \Phi$ if the particle is not lifted and $\phi < \Phi$ if it is lifted. Recalling that $\beta = a\ \sin\ \Phi\ \cos\ \theta_0$, see Fig. 3, the coordinates of the sphere center at time $t=0$, that is O_0, are

$$(0, \beta\ \tan\ \theta_0 = a\ \sin\ \Phi\ \sin\ \theta_0, a(1+\varepsilon) = \delta + a\ \cos\ \Phi).$$

The impact position of the incoming rolling particle relative to the peak is represented by angle θ_0. The relevant quantity for representing the impact is the distance between H_0' (projection of O_0 onto the xy plane, see Fig. 3) and the x-axis, that is $\beta\ \tan\ \theta_0$. The normalized distance

$$\mathcal{I} = \frac{\beta\ \tan\ \theta_0}{\lim_{\theta_0 \to \pi/2} \beta\ \tan\ \theta_0} = \sin\ \theta_0 \tag{62}$$

then appears as an "impact factor"', which varies from 0 for head-on collision with the peak ($\theta_0 = 0$) to unity for a "grazing" collision ($\theta_0 = \pi/2$).

During the sphere motion, when lifted the angle ϕ decreases from Φ possibly down to $\phi = 0$ whenever the sphere center is on the top of the peak. Finally, let us define the angle ψ of rotation around axis x_1, with its orientation such that ψ increases if the sphere rolls on the wall (with $\psi = 0$ at $t=0$). With this definition, we have $\Omega_1 = -\frac{\mathrm{d}\psi}{\mathrm{d}t}$.

Equation (46) is a condition for the onset of lifting of a particle rolling either without or with slip on the wall. Now, for the particle to actually be lifted, the aerodynamic force and torque should be such that:

$$\frac{C_2}{a} - n_3F_1 - n_1W \geq 0. \tag{63}$$

We now use the expressions for the aerodynamic force $F_1 = F_1^{\mathrm{s}} + F_1^{\mathrm{q}}$ and torque $C_2 = C_2^{\mathrm{s}} + C_2^{\mathrm{q}}$, taking into account (13) and (14). Since at the onset of lifting the particle is in contact with the rough wall, the lubrication formulae (15) apply for the

friction factors. The condition (63) then gives, with the change of frame (61):

$$(1.3213+1.9430\ \cos\ \Phi)\ \cos\ \theta\, K_q+(0.6293+1.7009\ \cos\ \Phi)\ \cos\ \theta-\sin\ \Phi\, \widetilde{V}_s \geq 0. \tag{64}$$

The components of the aerodynamic force and torque responsible for lifting the sphere around point P are, using (61):

$$(\mathbf{F}^{\mathrm{s}}+\mathbf{F}^{\mathrm{q}})\cdot\mathbf{e}_1=(F^{\mathrm{s}}+F^{\mathrm{q}})\ \cos\ \theta, \tag{65a}$$

$$(\mathbf{C}^{\mathrm{s}}+\mathbf{C}^{\mathrm{q}})\cdot\mathbf{e}_2=(C^{\mathrm{s}}+C^{\mathrm{q}})\ \cos\ \theta. \tag{65b}$$

They are larger for smaller θ, that is when the particle first comes in contact with point P at $\theta=\theta_0$. Indeed at later times, if it is not lifted, the particle may roll on the wall around the peak and θ then increases.

If the particle is lifted, its subsequent motion is three-dimensional since it turns around the peak while climbing on it. With the preceding notation, the equations of motion (60a)–(60c) of the lifted particle are in dimensionless form, using the reduced time $\widetilde{t}=k_{\mathrm{s}}t$, reduced velocities $\widetilde{U}_2=U_2/(k_{\mathrm{s}}a)$, $\widetilde{\Omega}_1=\Omega_1/k_{\mathrm{s}}$ and the dimensionless constant $\widetilde{k}_{\mathrm{q}}$ (3),

$$\frac{\mathrm{d}\theta}{\mathrm{d}\widetilde{t}}=\widetilde{U}_2 \tag{66a}$$

$$\begin{aligned}\mathrm{S_{tk}}\frac{\mathrm{d}\widetilde{U}_2}{\mathrm{d}\widetilde{t}}=&\left(\frac{20}{21}\cos\ \phi\ \sin\ \theta\, c^{\mathrm{q}}_{yx}\frac{\ell}{a}+\frac{5}{7}\sin\ \theta\, f^{\mathrm{q}}_{xx}\left(\frac{\ell}{a}\right)^2\right)\widetilde{k}_{\mathrm{q}}+\left(\frac{20}{21}\cos\ \phi\ \left(c^{\mathrm{r}}_{yy}-c^{\mathrm{r}}_{zz}\right)-\frac{5}{7}f^{\mathrm{r}}_{xy}\right)\widetilde{\Omega}_1\\&+\left(\frac{20}{21}\cos\ \phi\, c^{\mathrm{t}}_{yx}-\frac{5}{7}f^{\mathrm{t}}_{xx}-\frac{20}{21}c^{\mathrm{r}}_{zz}\right)\widetilde{U}_2+\frac{5}{7}\sin\ \theta\, f^{\mathrm{s}}_{xx}\frac{\ell}{a}+\frac{10}{21}\cos\ \phi\ \sin\ \theta\, c^{\mathrm{s}}_{yx}\end{aligned} \tag{66b}$$

$$\frac{\mathrm{d}\psi}{\mathrm{d}\widetilde{t}}=-\widetilde{\Omega}_1 \tag{66c}$$

$$\begin{aligned}\mathrm{S_{tk}}\frac{\mathrm{d}\widetilde{\Omega}_1}{\mathrm{d}\widetilde{t}}=&\left(\frac{50}{21}\cos^2\phi\ \sin\ \theta\, c^{\mathrm{q}}_{yx}\frac{\ell}{a}-\frac{5}{7}\cos\ \phi\ \sin\ \theta\, f^{\mathrm{q}}_{xx}\left(\frac{\ell}{a}\right)^2-\frac{10}{3}\sin\ \theta\, c^{\mathrm{q}}_{yx}\frac{\ell}{a}\right)\widetilde{k}_{\mathrm{q}}+\left(\frac{50}{21}\cos^2\phi\ \left(c^{\mathrm{r}}_{yy}-c^{\mathrm{r}}_{zz}\right)+\frac{5}{7}\cos\ \phi\, f^{\mathrm{r}}_{xy}-\frac{10}{3}c^{\mathrm{r}}_{yy}\right)\widetilde{\Omega}_1\\&+\left(\frac{5}{7}\cos\ \phi\, f^{\mathrm{t}}_{xx}-\frac{10}{3}c^{\mathrm{t}}_{yx}-\frac{50}{21}\cos\ \phi\, c^{\mathrm{r}}_{zz}+\frac{50}{21}\cos^2\phi\, c^{\mathrm{t}}_{yx}\right)\widetilde{U}_2+\frac{25}{21}\cos^2\ \phi\ \sin\ \theta\, c^{\mathrm{s}}_{yx}-\frac{5}{7}\cos\ \phi\ \sin\ \theta\, f^{\mathrm{s}}_{xx}\frac{\ell}{a}-\frac{5}{3}\sin\ \theta\, c^{\mathrm{s}}_{yx}\end{aligned} \tag{66d}$$

$$\frac{\mathrm{d}\phi}{\mathrm{d}\widetilde{t}}=-\widetilde{\Omega}_2 \tag{66e}$$

$$\begin{aligned}\mathrm{S_{tk}}\frac{\mathrm{d}\widetilde{\Omega}_2}{\mathrm{d}\widetilde{t}}=&\left(\frac{20}{21}\cos\ \theta\, c^{\mathrm{q}}_{yx}\frac{\ell}{a}+\frac{5}{7}\cos\ \phi\ \cos\ \theta\, f^{\mathrm{q}}_{xx}\left(\frac{\ell}{a}\right)^2\right)\widetilde{k}_{\mathrm{q}}+\left(\frac{20}{21}\cos\ \phi\, c^{\mathrm{t}}_{yx}-\frac{5}{7}\cos^2\phi\, f^{\mathrm{t}}_{xx}+\frac{5}{7}\cos\ \phi\, f^{\mathrm{r}}_{xy}-\frac{5}{7}\sin^2\phi\, f^{\mathrm{t}}_{zz}-\frac{20}{21}c^{\mathrm{r}}_{yy}\right)\widetilde{\Omega}_2\\&-\frac{5}{7}\sin\ \phi\, \widetilde{V}_s+\frac{5}{7}\cos\ \phi\ \cos\ \theta\, f^{\mathrm{s}}_{xx}\frac{\ell}{a}+\frac{10}{21}\cos\ \theta\, c^{\mathrm{s}}_{yx}.\end{aligned} \tag{66f}$$

The initial conditions (at $\widetilde{t}=0$) are:

$$\theta=\theta_0 \tag{67a}$$

$$\widetilde{U}_2=\frac{\mathrm{d}\theta}{\mathrm{d}\widetilde{t}}=\widetilde{U}_x\ \cos\ \theta_0 \tag{67b}$$

$$\psi=0 \tag{67c}$$

$$\widetilde{\Omega}_1=-\frac{\mathrm{d}\psi}{\mathrm{d}\widetilde{t}}=-\widetilde{\Omega}_y\ \cos\ \theta_0 \tag{67d}$$

$$\phi=\Phi \tag{67e}$$

$$\widetilde{\Omega}_2=-\frac{\mathrm{d}\phi}{\mathrm{d}\widetilde{t}}=0, \tag{67f}$$

with the two alternative cases:

- rolling without slip: $\widetilde{U}_x$ given by (26) and $\widetilde{\Omega}_y=\widetilde{U}_x$;
- rolling with slip: $\widetilde{U}_x$ given by (30b) and $\widetilde{\Omega}_y$ given by (30d).

As mentioned above, we consider $\theta_0>0$ (the case $\theta_0<0$ is simply a symmetry with respect to the plane $y=0$). Then θ increases from θ_0 to $\pi/2$, ψ increases from 0 and ϕ decreases from Φ.

When θ increases during the trajectory, the force and torque (65) responsible for lifting the particle decrease. It may then be possible that the particle is not fully lifted, depending on the various physical parameters. That is, ϕ decreases from Φ down to some value which may be $\phi > 0$. If the particle has been little lifted during its motion around the peak, it will be submitted to a low ambient flow velocity and will subsequently progress at a small distance from the wall with a low velocity. On the other hand, if the particle is lifted to the top of the peak, when ϕ has decayed to zero, it will be submitted to a higher velocity of the ambient shear flow and will thereafter progress faster, at a larger distance from the wall. The motion along z of the particle after leaving the peak P will be considered at the end of the next subsection, Section 6.3.

The spherical particle stays in contact with the point P until either component P_1 or P_3 of the force in P vanishes. We obtain with (60d) and (60f) the following dimensionless expressions:

$$\widetilde{P}_1 = \frac{P_1}{6\pi a^2 \mu k_s} \tag{68a}$$

$$\begin{aligned}\widetilde{P}_1 = {} & \left[\frac{20}{21}\cos\Phi\cos\theta\, c^{q}_{yx}\left(\frac{\ell}{a}\right) - \cos\theta\, f^{q}_{xx}\left(\frac{\ell}{a}\right)^2 + \frac{5}{7}\cos^2\Phi\cos\theta\, f^{q}_{xx}\left(\frac{\ell}{a}\right)^2\right] K_q \\ & + \left[\frac{20}{21} c^{t}_{yx}\cos^2\Phi - \frac{20}{21}\cos\Phi\, c^{r}_{yy} + \frac{5}{7}\cos^3\Phi\, f^{t}_{zz} + f^{t}_{xx}\cos\Phi - \frac{5}{7}\cos^3\Phi\, f^{t}_{xx} - \frac{5}{7}\cos\Phi\, f^{t}_{zz} - f^{r}_{xy} + \frac{5}{7}\cos^2\Phi\, f^{r}_{xy}\right]\widetilde{\Omega}_2 \\ & - \cos\theta\, f^{s}_{xx}\left(\frac{\ell}{a}\right) - \frac{5}{7}\cos\Phi\sin\Phi\,\widetilde{V}_s + \frac{5}{7}\cos^2\Phi\cos\theta\, f^{s}_{xx}\left(\frac{\ell}{a}\right) + \frac{10}{21}\cos\Phi\cos\theta\, c^{s}_{yx}\end{aligned} \tag{68b}$$

$$\widetilde{P}_3 = \frac{P_3}{6\pi a^2 \mu k_s} \tag{68c}$$

$$\begin{aligned} = {} & \left[\frac{2}{7} + \frac{5}{7}\cos^2\Phi\right]\widetilde{V}_s + \left[\frac{5}{7}\cos\Phi\sin\Phi\cos\theta\, f^{q}_{xx}\left(\frac{\ell}{a}\right)^2 + \frac{20}{21}\sin\Phi\cos\theta\, c^{q}_{yx}\left(\frac{\ell}{a}\right)\right] K_q \\ & + \left[\frac{20}{21}\sin\Phi\, c^{t}_{yx}\cos\Phi - \frac{20}{21}\sin\Phi\, c^{r}_{yy} - \frac{5}{7}\cos^2\Phi\sin\Phi\, f^{t}_{xx} + \frac{5}{7}\cos\Phi\sin\Phi\, f^{r}_{xy} + \frac{2}{7} f^{t}_{zz}\sin\Phi + \frac{5}{7} f^{t}_{zz}\sin\Phi\cos^2\Phi\right]\widetilde{\Omega}_2 \\ & + \frac{5}{7}\cos\Phi\sin\Phi\cos\theta\, f^{s}_{xx}\left(\frac{\ell}{a}\right) + \frac{10}{21}\sin\Phi\cos\theta\, c^{s}_{yx}. \end{aligned} \tag{68d}$$

The equations in this section will be used in Section 7 to calculate the particle trajectories.

6.3. *Free motion of particle after leaving the peak*

Here, it should be recalled that when the particle leaves the peak, it is not lifted by the fluid since there is no lift force in Stokes flow. Yet, after leaving the peak, the preceding upward motion may continue while decaying during a time of order τ_p, Eq. (7), due to particle inertia. The motion along z is considered here.

Using the appropriate dimensionless quantities defined in Appendix B.2, the equation of motion for the sphere center along z is (B.8), with (B.7). The particle leaves the peak at a position Z_1 with a vertical velocity $\hat{U}_{z1}$ obtained from (55) with $\Omega_2 = -\mathrm{d}\phi/\mathrm{d}t$ and $n_1 = \sin\phi$, that is:

$$\hat{U}_{z1} = -\left[\sin\phi\,\frac{\mathrm{d}\phi}{\mathrm{d}\hat{t}}\right]_1,$$

where $[\,]_1$ denotes quantities calculated at this time when the particle leaves the peak. The differential system (B.7)–(B.8) is integrated from Z_1 up to the position Z_m where the particle velocity eventually vanishes because of the viscous dissipation and the particle weight.

7. Calculation of lifted particle trajectories

The differential system (66) with initial conditions (67) is integrated numerically. Since the aerodynamic force and torque become singular in the limit $\varepsilon \to 0$, the differential system is stiff. We then use for integration a predictor–corrector technique, that is more appropriate than e.g. a Runge–Kutta scheme which could not converge.

Table 1
Typical cases chosen for the calculation of trajectories in Section 7; d is the particle diameter and W_A is the adhesion force.

Case	d (μm)	W_A (nN)
(i)	5	1
(ii)	20	20
(iii)	40	40

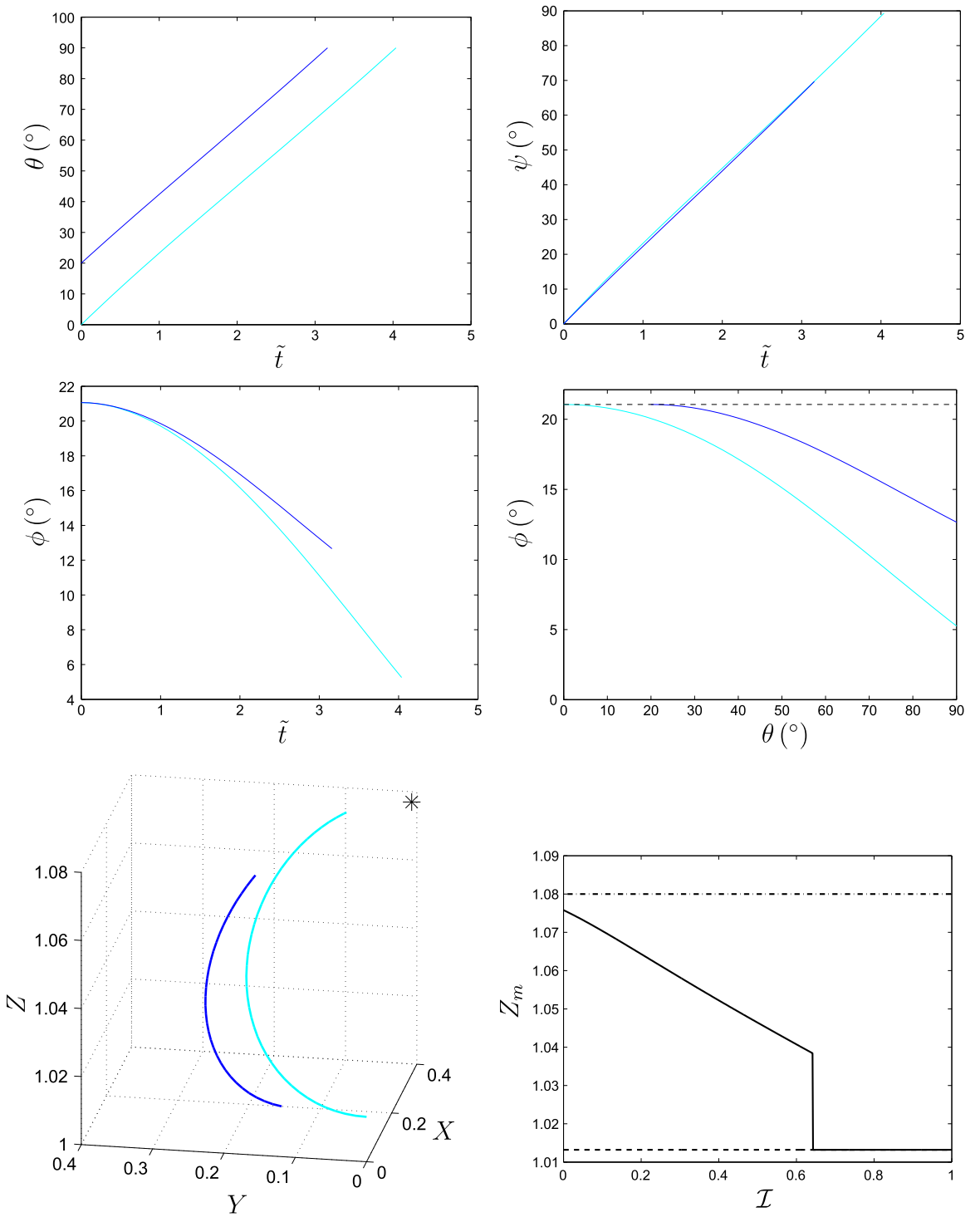

Fig. 4. Data of case (i). Evolution of angles θ, ψ, ϕ versus dimensionless time $\widetilde{t}$, trajectories in (ϕ, θ) plane and three-dimensional particle trajectories in (X, Y, Z) frame during particle lifting. The angle ϕ is starting here from $\Phi = 21.06^\circ$. The two trajectories correspond to $\theta_0 = 0^\circ, 20^\circ$ (cyan, blue, respectively). Bottom, right: maximum dimensionless distance from the rough wall when leaving the peak, Z_m, versus the impact factor $\mathcal{I}$. The lower dashed line corresponds to a particle on the rough wall and the upper dash-dotted line to a particle that would be sitting on the top of the peak.

Calculations are performed in this section for alumina particles lifted from an epoxy wall, values of the adhesion forces and wall roughness being given in Section 3.3. The density of alumina is 3900 kg/m^3. The density and viscosity of air are taken as 1.3 kg/m^3 and 1.8×10^{-5} Pa · s, respectively. The shear rate of the ambient shear flow is $k_s = 10^5\ s^{-1}$ and the curvature of the ambient shear flow is assumed to be zero.

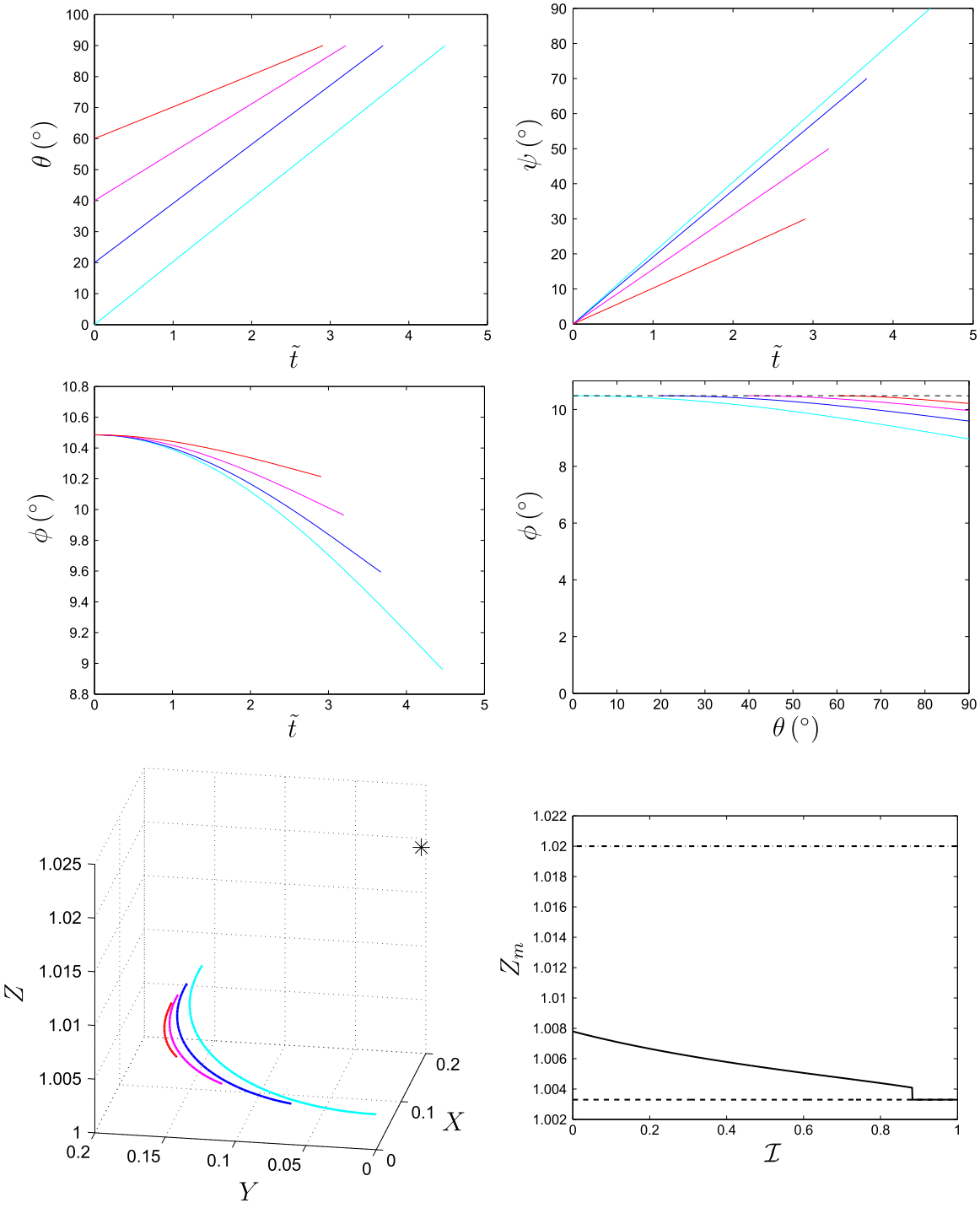

Fig. 5. Same as Fig. 4 for the data of case (ii). The angle ϕ is starting here from $\Phi = 10.49°$. The four trajectories correspond to $\theta_0 = 0°, 20°, 40°, 60°$ (cyan, blue, magenta, red, respectively).

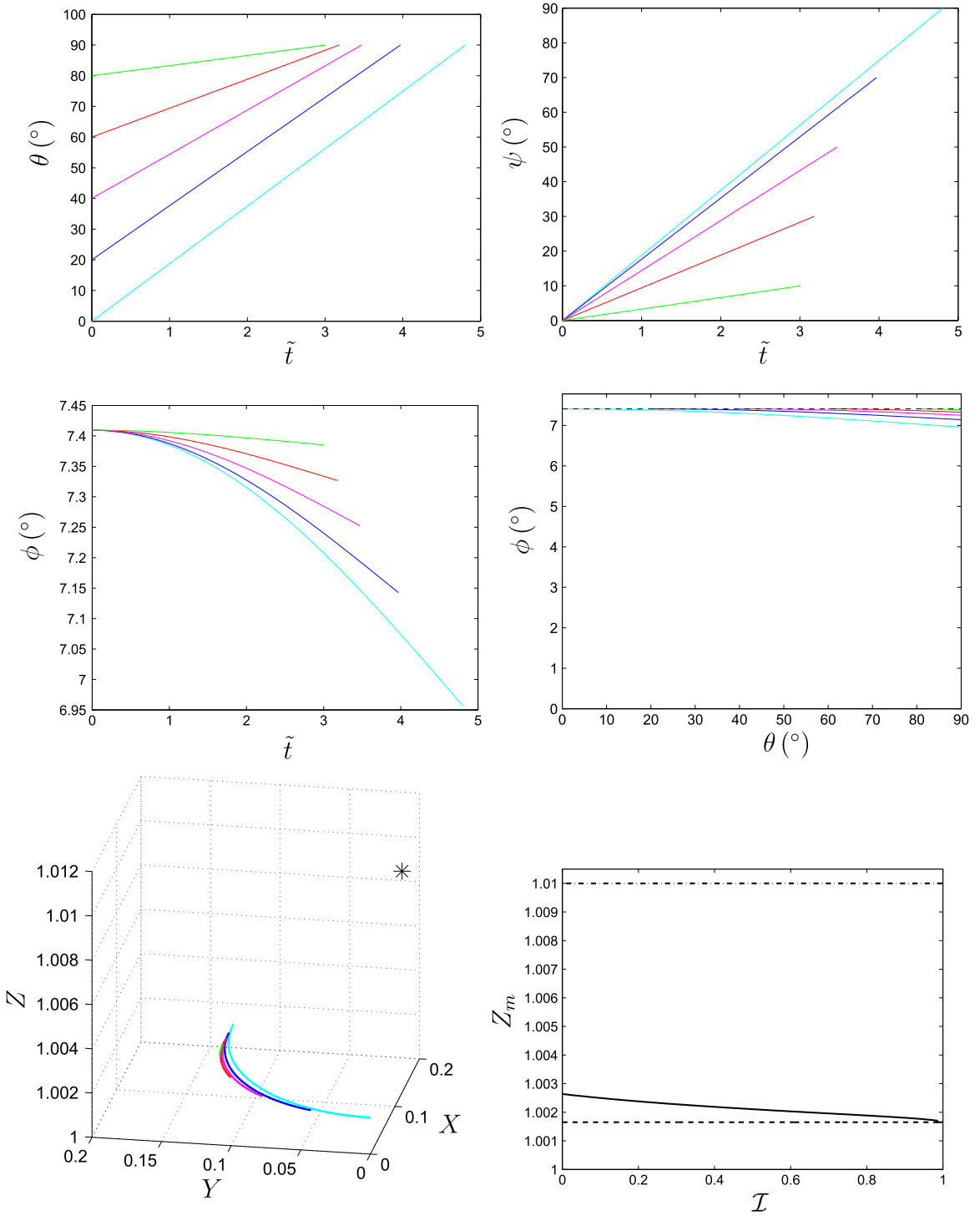

Fig. 6. Same as Fig. 4 for the data of case (iii). The angle ϕ is starting here from $\Phi = 7.41°$. The five trajectories correspond to $\theta_0 = 0°, 20°, 40°, 60°, 80°$ (cyan, blue, magenta, red, green, respectively).

We study here the influences of the particle diameter $d=2a$ and of the adhesion force. Numerical results show that particles with $d=5$ μm and an adhesion force of $W_A=18$ nN (that is the median of the measured adhesion force distribution, Appendix A) are not lifted by the airflow. We then consider the case of a weak adhesion force, $W_A=1$ nN, corresponding to the lower part of the measured adhesion force distribution for these particles, see Section 3.3 and Appendix A (in particular Fig. A3). Larger particles are subjected to a higher aerodynamic force and can be lifted even for a higher adhesion force. Some typical results are shown in the following figures. They concern the cases shown in Table 1.

From the measurements in Appendix A, we consider a peak of height $\delta=200$ nm. We then calculate

$$\Phi=\text{arc cos}\left(1+\varepsilon-\frac{2\delta}{d}\right)$$

Calculations of trajectories were performed for the following initial conditions:

$$\theta_0=0^\circ,20^\circ,40^\circ,60^\circ,80^\circ,$$

corresponding respectively to an impact factor, Eq. (62), of

$$0,0.34,0.64,0.87,0.98.$$

The presented curves are only those for which the sphere is lifted from the surface. Therefore, there are sometimes no curves for some large values of θ_0, when the aerodynamic force and torque are too small for lifting the sphere. The following curves for trajectories are presented in each figure:

- angle θ versus the normalized time $\widetilde{t}$,
- angle ψ versus the normalized time $\widetilde{t}$,
- angle ϕ versus the normalized time $\widetilde{t}$,
- angle ψ versus the angle θ,
- trajectory of the sphere center in dimensionless coordinates

$$X=x/a,\quad Y=y/a,\quad Z=\ell/a.$$

Recall that the origin $X=0$ is defined as the abscissa of the sphere center in the $Y=0$ plane when the sphere is in contact with the peak P. The position for which the sphere center would be on the top of the peak, that is $(0,\ \sin\ \Phi, 1+\delta/a)$, is represented by a star.

After the particle has left the peak, the final distance to the wall is calculated as explained in Section 6.3. Practically, the velocity vertical velocity $\hat{U}_{z1}$ when leaving the peak is so small that the drag force is negligible as compared with the gravity term in (B.8). Thus the inertial motion is ballistic parabolic. Then, the maximum vertical inertial displacement of the particle is found to be negligible. That is, particles after leaving the peak stay practically at the same distance from the wall. The lower right plot in each figure (Figs. 4–6) shows the maximum distance $Z_m\simeq Z_1$ versus the impact factor $\mathcal{I}$, for θ_0 varying from 0 to 90°. Trajectories were calculated by steps of 0.1°. The lower dashed line represents the position of the center of a particle that would stay on the wall. The top dash-dotted line represents the position of a particle that would be lifted to the top of the peak. The solid line represents Z_m.

For cases (i), (ii), (iii) ($d=5,20,40$ μm), there are respectively 2, 4, 5 lifted trajectories. Note that the lifted trajectories starting at $\theta_0=0^\circ$ are in the $Y>0$ half-space because the starting point is actually for a very small positive θ_0.

For case (i), Fig. 4, the shown lifted trajectories are for $\theta_0=0^\circ$ and $\theta_0=20^\circ$. Those for $\theta_0=40,60,80^\circ$ are not lifted. More precisely, all trajectories for $\theta_0\geq 40.0^\circ$ are not lifted; in the Z_m versus $\mathcal{I}$ plot, the discontinuity is at $\mathcal{I}=\sin 40.0^\circ=0.643$. The trajectory starting at $\theta_0=0^\circ$ is nearly lifted to the top of the peak (as marked by a star in the (X,Y,Z) plot). The maximum absolute displacement is 157 nm. For the shear rate $k_s=10^5\ \text{s}^{-1}$ that we are considering, the ambient shear flow at the sphere center is 25 cm/s on the wall and is then increased of 1.56 cm/s, which is moderate.

For case (ii), Fig. 5, the shown lifted trajectories are for $\theta_0=0,20,40,60^\circ$. More precisely, all trajectories for $\theta_0\geq 62.0^\circ$ (that is for $\mathcal{I}=0.883$) are not lifted. The lifted trajectories attain a much lower Z_m than for case (i). The maximum absolute displacement is 45 nm, giving an increase in ambient flow velocity of 0.45 cm/s.

For case (iii), Fig. 6, all five calculated trajectories, for $\theta_0=0,20,40,60,80^\circ$, are lifted. More precisely, all trajectories for $\theta_0\geq 80.3^\circ$ are not lifted. Since this corresponds to $\mathcal{I}=0.986$, it can be said that practically all particles are lifted. The attained Z_m is very low. The maximum absolute displacement is 20 nm (that is of the order of the mean roughness), giving an increase in ambient flow velocity of 0.20 cm/s.

In all plots representing Z_m versus $\mathcal{I}$, it is found that there is a discontinuity for some value of $\mathcal{I}$, depending on the particle size. Surprisingly, the function $Z_m(\mathcal{I})$ for lifted particles is nearly linear. These last plots are useful for entrainment of particles by the air flow.

The conclusion is that the smaller particles are more easily lifted and then submitted to a (moderately) higher ambient flow. This is because even though larger particles are submitted to a higher drag force and torque by the air flow, their upward motion is impeded by their weight.

Case (i) concerns an adhesion force of $W_A=1$ nN which is the lower bound found in the experimental range. But if the adhesion force is increased only up to $W_A=1.4$ nN, the particle is not lifted at all. In all presented cases, it is found that the

particle rolls without slipping on the wall before encountering the peak. Trying $d = 40$ μm with a lower adhesion force, $W_A = 20$ nN instead of $W_A = 40$ nN, it is found that the particle slips while rolling on the wall before encountering the peak. Thereafter, there are also five up-lifted trajectories. Then, the maximum attained Z_m is lower: 1.0020 instead of 1.0026.

For a higher peak of 300 nm (figures not shown here), a particle of diameter 5 μm has one lifted trajectory starting at $\theta_0 = 0$; it is displaced up to 228 nm and is then submitted to an increase in ambient flow velocity of 2.28 cm/s. For $\theta_0 \geq 8.4^\circ$, the particle is not lifted. A particle of diameter 20 μm has 3 lifted trajectories with a maximum displacement of 57 nm and one of $d = 40$ μm has 5 lifted trajectories with a maximum displacement of 25 nm. Thus, for a higher peak, there are less lifted trajectories for the small particle but the displacement is significantly higher. For the larger particles, there are as many lifted trajectories and the displacement is similar.

In all cases, for a lower/higher adhesion force and for a lower/higher peak, there would be more/less climbing trajectories. The few examples presented here show in particular the sensitivity to the adhesion force.

8. Conclusion

A model is proposed for the three-dimensional motion of a small particle moving in a gas near a rough wall and encountering a peak of roughness.

Before the encounter, it is considered that the particle is in contact with a rough wall and moves due to the applied aerodynamic force and torque of the ambient shear flow. The aerodynamic stresses are expressed in terms of earlier accurate results calculated in the frame of Stokes equations of fluid motion. Conditions are found for the particle either to roll without slip or with slip.

When the particle encounters the peak of roughness, the problem is found to be undetermined. When the particle does not slip on the wall, the problem is hyperstatic in the plane normal to the contact plane and containing the particle center and the peak. This problem is discussed in detail. When the particle slips on the wall, it is considered that the problem cannot be hyperstatic in the plane just mentioned, but rather that a dynamic friction applies. Then, for both the no-slip and slip cases, conditions for the particle to be lifted are obtained. Trajectories of the particle when lifted and moving around the peak are calculated. Even though fluid inertia is negligible, it is expected that particle inertia might be important and it is taken into account in the calculations.

The adhesion force between the particle and the rough wall is measured for micrometer sized alumina particles and a substrate made of epoxy resin. Using an alumina particle glued on the tip of the cantilever of an Atomic Force Microscope (see Appendix A) allows us to measure both the substrate roughness and the adhesion force with the same apparatus.

Some typical cases of a particle encountering a peak are presented as examples. Calculated trajectories show that the particle may or may not be lifted, and when lifted rotate around the peak while climbing, depending on the adhesion forces and the various aerodynamic parameters. It is interesting to note that the smallest considered particles are the most displaced ones when leaving the peak. For the examples calculated here, it is found that particles are practically not lifted by their inertia after leaving the peak (the lift force due to fluid inertia is neglected here in the framework of Stokes equations). Eventually, the farther it is from the wall, the faster a particle is entrained by the ambient shear flow. Considering the large number of isolated peaks, see Fig. 2, their global effect is eventually quite significant during particle motion.

Thus, determining the three-dimensional trajectory around the peak is essential in assessing the subsequent particle entrainment by the ambient shear flow.

These few examples show the richness of possible behaviors contained in the modeling equations for particle lifting. This model may be used as a basis for calculating particle motion close to a rough wall in various applications.

Acknowledgments

F.F. acknowledges the support of IRSN, grant number RE35/12016622.

Appendix A. Measurement of substrate roughness and particle adhesion force using atomic force microscope (AFM)

The topography of surfaces and particle adhesion forces were measured with an atomic force microscope (AFM) model *Multimode 8 Nanoscope V*, by *Bruker*. The AFM operates in *Tapping mode* for substrate roughness characterization and in *PeakForce*^{TM}*–QNM*^{TM} for particle adhesion force measurement.

A.1. Measurement of substrate roughness

In tapping mode, the cantilever oscillates and a sufficiently high oscillation amplitude is selected for the tip to pass through the contamination layer that is usually present on the analyzed surfaces. The tip comes into contact with the surface only periodically. An analysis in tapping mode therefore allows a topographical surface study without disturbance of the sample, in particular by eliminating frictional forces.

The analysis is performed at constant amplitude, which means that the variation of the oscillation amplitude of the tip is used as a control signal in order to correct the z-displacement to keep the amplitude constant and follow the topography of the surface.

Figure A1 represents two topographic images of the surface. The left-hand-side is an image of a $50 \times 50\ \mu m^2$ surface area with a full scale in height of 0.2 μm represented by a color code. The right-hand-side is a $100 \times 100\ \mu m^2$ surface area with a full scale in height of 0.4 μm. The roughness parameters corresponding to the analysis of the $100 \times 100\ \mu m^2$ surface area sample are Rq = 77.3 nm, Ra = 32.1 nm, Rdiff = 3%. Rq is the standard deviation of the height measurement, Ra is the mean

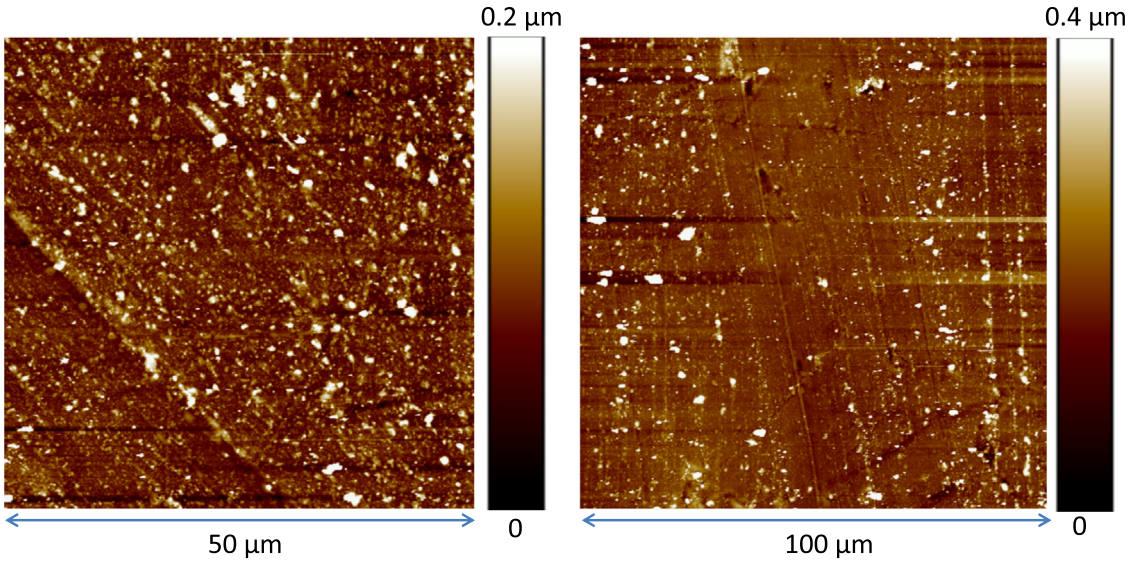

Fig. A1. Topographic images of the surface of a 1 mm thick layer of epoxy resin glued on a concrete substrate.

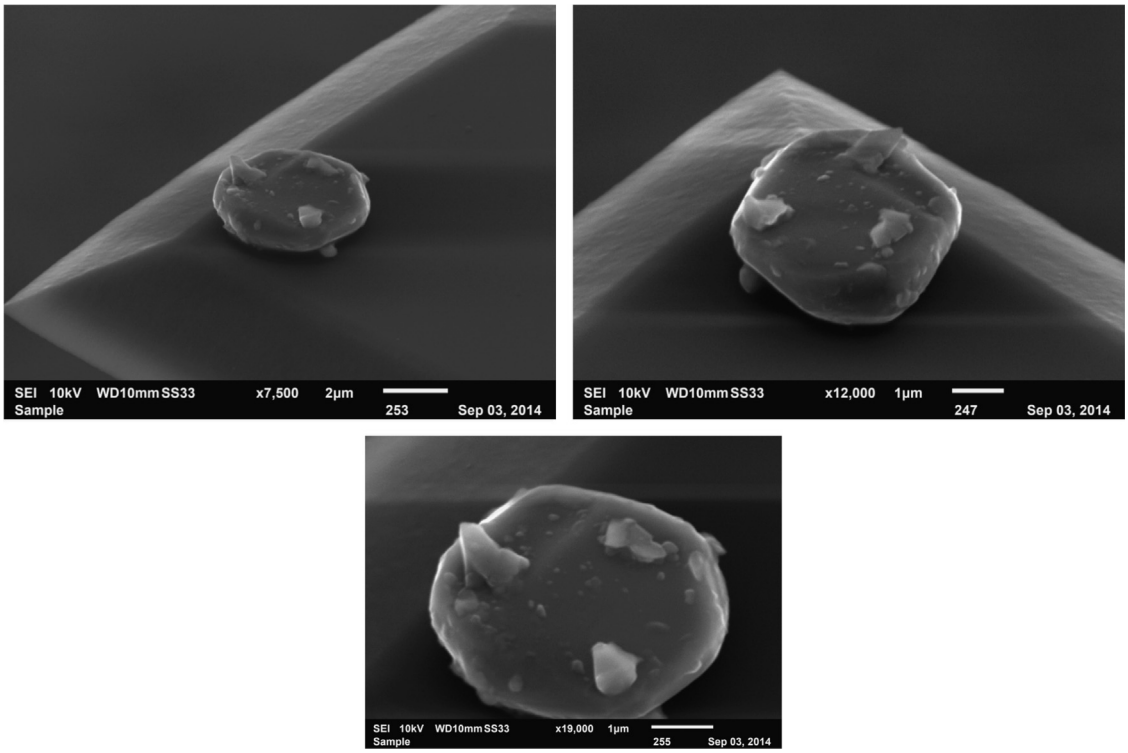

Fig. A2. Scanning electron micrographs of a 5 μm alumina particle stuck on the tip of an AFM cantilever. The pictures show the same particle with different magnifications and viewing angles.

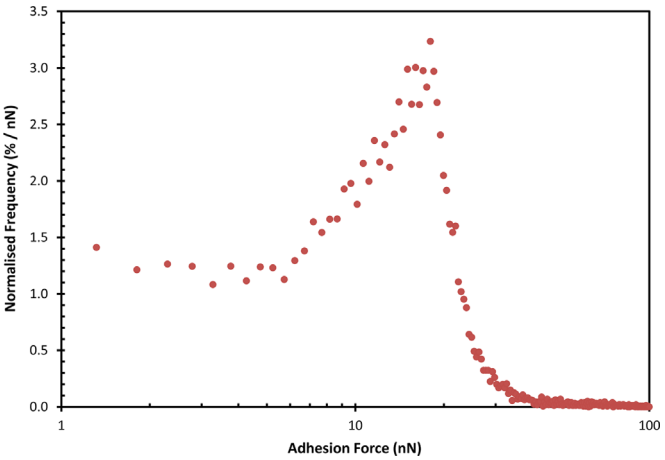

Fig. A3. Adhesion force distribution for a 5 μm alumina particle on an epoxy substrate.

roughness corresponding to the distance between planes defined by the mean and median height values. Rdiff is the percentage of surface increase between the developed surface (calculated by triangulation) and the swept surface.

The topographic images of the surface reveal many isolated white spots. According to the full scale in height, white spots correspond to peaks with a height larger than 0.2 μm on the left-hand-side image and larger than 0.4 μm on the right-hand-side one. Images and values of the roughness parameters show that between the peaks the surface is relatively smooth, with $Ra < 0.1$ μm.

A.2. Measurement of particle adhesion force

Over the past few decades, many techniques have been developed to characterize particle-surface adhesion: electric field detachment, centrifugal detachment and Atomic Force Microscopy (AFM) (Mizes, Ott, Eklund, & Hays, 2000). AFM can accurately and precisely measure the adhesion of single particles on a surface (Burnham, Colton, & Pollock, 1993) and recent works were published on the benefit of this technique in the field of particle resuspension (Walker et al., 2010; Pecault, Gensdarmes, Basso, & Sommer, 2012; Mokgalapa, Ghosh, & Loyalka, 2014; Tan, Gao, Wee, & Asa-Awuku, 2014). To measure the adhesion force between an alumina particle and an epoxy substrate, the particle is stuck on the cantilever of an AFM. The stiffness constant of the cantilever in our experiments is around 2.8 N/m. A scanning electron micrograph of an alumina particle stuck on the tip of the cantilever is shown in Fig. A2. The particle equivalent diameter in terms of equivalent projected surface area is 4.5 μm. The particle exhibits some large asperities on its surface with size up to one micrometer.

A force curve is obtained in Peak force mode by applying a sinusoidal voltage (along the z axis) to the piezoelectric ceramic element, which then either extends to contact between the tip and the surface or to a value set by the operator (trigger), and then retracts, approaching and separating the sample and the probe tip. A typical force curve is shown by Pecault et al. (2012).

Here we present as an example the statistical analysis of the results of the measurement of an adhesion force distribution between the 5 μm alumina particle shown in Fig. A2 and the epoxy resin substrate whose roughness is represented in Fig. A1. For each experiment, the substrate was new and cleaned with propanol. The distribution of the adhesion force is obtained by scanning a surface area of 50×50 μm^2 on which 4096 values of the force are measured. Figure A3 represents the obtained normalized distribution.

Values of the adhesion force distribution range from 1 nN to 40 nN with a median value of 18 nN. The distribution does not exhibit a log-normal shape as frequently reported in the literature for spherical particles on a rough surface (Biasi, De Los Reyes, Reeks, & De Santi, 2001). The peculiar force distribution obtained here is probably due to the shape of the particle with asperities on its surface. The median value of the force is lower than that calculated for a 5 μm particle using the empirical correlation proposed by Biasi et al. (2001) for resuspension assessment. The Biasi et al. median value is equal to 80 nN with a spectrum of the distribution force ranging from 10 nN to 500 nN. The low adhesion value obtained in our case is probably due to the asperities on the particle which increase the distance between the bulk particle and the surface at contact. Nevertheless it provides an order of magnitude of the adhesion for a particle and a surface of interest in our application. Further experiments are planned in order to obtain data for a complete panel of particle shapes.

Appendix B. Bouncing of a particle on a large peak

Consider here the case when the particle collision with the peak is elastic.

B.1. Bouncing velocity

The impact velocity of the particle is along the x-axis: $\mathbf{U}=U_x\mathbf{i}$. Thus, in the reference frame (x_1,x_2,x_3), see Fig. 3, it is:

$$\mathbf{U}=(\mathbf{e}_1\ \cos\ \theta+\mathbf{e}_2\ \sin\ \theta)\,U_x. \tag{B.1}$$

The bouncing velocity of the particle on the peak,

$$\mathbf{U}'=U'_1\mathbf{e}_1+U'_2\mathbf{e}_2+U'3\mathbf{e}_3, \tag{B.2}$$

is related to the impact velocity $\mathbf{U}=U_1\mathbf{e}_1+U_2\mathbf{e}_2$, by:

$$U'_1\mathbf{e}_1+U'_3\mathbf{e}_3=U_1\mathbf{e}_1-2(U_1\mathbf{e}_1\cdot\mathbf{n})\mathbf{n}, \tag{B.3a}$$

$$U'_2\mathbf{e}_2=U_2\mathbf{e}_2. \tag{B.3b}$$

Using the angle $\Phi=\widehat{HOP}$ (see Fig. 1, Fig. 3),

$$\mathbf{n}=\mathbf{e}_1\ \sin\ \Phi-\mathbf{e}_3\ \cos\ \Phi. \tag{B.4}$$

From (B.1)–(B.4), we derive:

$$\mathbf{U}'=U_x(\mathbf{e}_1\ \cos\ 2\Phi\ \cos\ \theta+\mathbf{e}_2\ \sin\ \theta+\mathbf{e}_3\ \sin\ 2\Phi\ \cos\ \theta),$$

that is, in the (x,y,z) frame:

$$\mathbf{U}'=U_x\{\mathbf{i}[1-\cos^2\theta\,(1-\cos\ 2\Phi)]+\mathbf{j}\ \sin\ \theta\ \cos\ \theta\,(1-\cos\ 2\Phi)+\mathbf{k}\ \cos\ \theta\ \sin\ 2\Phi\}. \tag{B.5}$$

B.2. Inertial vertical motion after elastic bouncing

Consider the vertical motion following the elastic rebound with initial velocity, from (B.5): $U'_{z0}=U_x\ \cos\ \theta\ \sin\ 2\Phi$. The corresponding kinetic energy is $E_c=\frac{1}{2}mU'^2_{z0}$. Note that the actual kinetic energy may be smaller if the collision is not elastic. In any case, for the particle to be lifted by the collision, the kinetic energy has to be high enough to overcome the particle adhesion energy to the wall, $E_A=\pi r_c^2\mathcal{E}_A$. Whenever this happens, the resulting vertical velocity after collision is:

$$U_{z0}=\sqrt{U'^2_{z0}-U_A^2} \tag{B.6}$$

where $U_A=\sqrt{2\pi r_c^2\mathcal{E}_A/m}$ has the dimension of a velocity.

To describe the subsequent inertial vertical motion of the particle, appropriate dimensionless quantities are the height $Z=\ell/a$, the time $\hat{t}=t/\tau_p$ where τ_p is defined in (7), and the vertical velocity $\hat{U}_z=U_z\tau_p/a$, so that:

$$\frac{\mathrm{d}Z}{\mathrm{d}\hat{t}}=\hat{U}_z. \tag{B.7}$$

The dimensionless equation for the vertical motion, including particle weight, is:

$$\frac{\mathrm{d}\hat{U}_z}{\mathrm{d}\hat{t}}=-f^{\mathrm{t}}_{zz}\hat{U}_z-\frac{\tau_p^2 g}{a}, \tag{B.8}$$

where g is the acceleration of gravity. Solving the differential system (B.7) and (B.8) with initial condition $\hat{U}_z=U_{z0}\tau_p/a$ at $Z=1+\varepsilon$ provides the particle trajectory. The maximum height attained following a head-on collision ($\theta=0$) and using the data of Section 7 is $Z_{max}=26.7, 25.0, 11$, for a particle of diameter $d=5, 20, 40\ \mu$m, respectively. Because of its weight, the particle thereafter falls back onto the wall. This is the so-called *saltation*.

References

Albert, R., Albert, I., Hornbaker, D., Schiffer, P., & Barabasi, A. (1997). Maximum angle of stability in wet and dry spherical granular media. *Physical Review E, 56*, R6271–R6274.

Biasi, L., De Los Reyes, A., Reeks, M., & De Santi, G. (2001). Use of a simple model for the interpretation of experimental data on particle resuspension in turbulent flows. *Journal of Aerosol Science, 32*, 1175–1200.

Boulaud, D., Gerasimo, P., Martin, G., Martinot, L., Nourreddine, A., & Sens, J. (2003). Evaluation of the resuspension factor of contamination in nuclear power installations. *Radioprotection, 38*, 493–508.

Bowden, F., & Tabor, D. (1950). *The friction and lubrication of solids*. Oxford: Clarendon.

Bretherton, F. P. (1962). The motion of rigid particles in a shear flow at low Reynolds number. *Journal of Fluid Mechanics, 14*, 284–304.

Brunskill, R., 1964. The relationship between surface and airborne contamination. In B. Fish (Ed.), *Surface contamination, proceedings of the symposium held at Gatlinburg, Tennessee, June 1964* (pp. 93–105). New-York: Pergamon Press.

Burnham, N., Colton, R., & Pollock, H. (1993). Interpretation of force curves in atomic force microscopy. *Nanotechnology, 4*, 64–80.

Chaoui, M., & Feuillebois, F. (2003). Creeping flow around a sphere in a shear flow close to a wall. *Quarterly Journal of Mechanics and Applied Mathematics*, *56*, 381–410 Corrigendum: 65, 4 (2012).
Cheng, W., Dunn, P. F., & Brach, R. M. (2002). Surface roughness effects on microparticle adhesion. *The Journal of Adhesion*, *78*, 929–965.
Choi, J.-I., Edwards, J., Rosati, J., & Eisner, A. (2012). Large eddy simulation of particle re-suspension during a footstep. *Aerosol Science and Technology*, *46*, 767–780.
Davis, R. H., Serayssol, J.-M., & Hinch, E. J. (1986). The elastohydrodynamic collision of two spheres. *Journal of Fluid Mechanics*, *163*, 479–497.
Ekiel-Jeżewska, M. L., Feuillebois, F., Lecoq, N., Masmoudi, K., Anthore, R., Bostel, F., & Wajnryb, E. (1999). Hydrodynamic interactions between two spheres at contact. *Physical Review E*, *59*, 3182–3191 Erratum: 60:4994 (1999).
Ekiel-Jeżewska, M. L., Lecoq, N., Anthore, R., Bostel, F., & Feuillebois, F. (2002). Rotation due to hydrodynamic interactions between two spheres at contact. *Physical Review E*, *66*, 1–14.
Feuillebois, F. (1989). Some theoretical results for the motion of solid spherical particles in a viscous fluid. In G. F. Hewitt, J. M. Delhaye, N. Zuber (Eds.), *Multiphase science and technology* (Vol. 4, pp. 583–798). New York: Hemisphere Publishing Co.
Gavze, E., & Shapiro, M. (1997). Particles effect in a shear flow near a solid wall: Effects of nonsphericity on forces and velocities. *International Journal of Multiphase Flow*, *23*, 155–182.
Gavze, E., & Shapiro, M. (1998). Motion of inertial spheroidal particles in a shear flow near a solid wall with special application to aerosol transport in microgravity. *Journal of Fluid Mechanics*, *371*, 59–79.
Goldasteh, I., Goodarz, A., & Ferro, A. (2013). Monte Carlo simulation of micron size spherical particle removal and resuspension from substrate under fluid flows. *Journal of Aerosol Science*, *66*, 62–71.
Goldman, A. J., Cox, R. G., & Brenner, H. (1967). Slow viscous motion of a sphere parallel to a plane wall. II. Couette flow. *Chemical Engineering Science*, *22*, 653–660.
Gomes, C., Freihaut, J., & Bahnfleth, W. (2007). Resuspension of allergen-containing particles under mechanical and aerodynamic disturbances from human walking. *Atmospheric Environment*, *41*, 5257–5270.
Guingo, M., & Minier, J.-P. (2008). A new model for the simulation of particle resuspension by turbulent flows based on a stochastic description of wall roughness and adhesion forces. *Journal of Aerosol Science*, *39*, 957–973.
Happel, J., & Brenner, H. (1973). *Low Reynolds number hydrodynamics*. Leyden: Noordhoff.
Hardy, W., & Bircumshaw, I. (1925). Boundary lubrication. Plane surfaces and the limitations of Amontons' Law. *Proceedings of the Royal Society of London Series A*, *108*(745), 1–27.
Ibrahim, A., Dunn, P., & Brach, R. (2003). Microparticle detachment from surfaces exposed to turbulent air flow: Controlled experiments and modeling. *Journal of Aerosol Science*, *34*, 765–782.
Jones, I., & Pond, S. (1964). Some experiments to determine the resuspension factor of plutonium from various surfaces. In B. Fish (Ed.), *Surface contamination, proceedings of the symposium held at Gatlinburg, Tennessee, June 1964* (pp. 83–92). New-York: Pergamon Press.
Kubota, Y., & Higuchi, H. (2013). Aerodynamic particle resuspension due to human foot and model foot motions. *Aerosol Science and Technology*, *47*, 208–217.
Lecoq, N., Anthore, R., Cichocki, B., Szymczak, P., & Feuillebois, F. (2004). Drag force on a sphere moving towards a corrugated wall. *Journal of Fluid Mechanics*, *513*, 247–264.
Mana, Z. (2014). *Étude de la remise en suspension de particules due à la marche d'un opérateur* (Ph.D. thesis). Université Paris-Sud. Rapport ISRN/IRSN/2015-176.
Mizes, H., Ott, M., Eklund, E., & Hays, D. (2000). Small particle adhesion: Measurement and control. *Colloid and Surfaces A: Physicochemical and Engineering Aspects*, *165*, 11–23.
Mokgalapa, N., Ghosh, T., & Loyalka, S. (2014). Graphite particle adhesion to hastelloy x: Measurements of the adhesive force with an atomic force microscope. *Nuclear Technology*, *186*, 45–59.
Oberoi, R., Choi, J.-I., Edwards, J., Rosati, J., Thornburg, J., & Rodes, C. (2010). Human-induced particle re-suspension in a room. *Aerosol Science and Technology*, *44*, 216–229.
O'Neill, M. E. (1968). A sphere in contact with a plane wall in a slow linear shear flow. *Chemical Engineering Science*, *23*, 1293–1298.
O'Neill, M. E., & Stewartson, K. (1967). On the slow motion of a sphere parallel to a nearby wall. *Journal of Fluid Mechanics*, *27*, 705–724.
Pasol, L., Sellier, A., & Feuillebois, F. (2006). A sphere in a second degree polynomial creeping flow parallel to a wall. *Quarterly Journal of Mechanics and Applied Mathematics*, *59*, 587–614.
Pasol, L., Sellier, A., & Feuillebois, F. (2010). Creeping flow around a solid sphere in the vicinity of a plane solid wall. In F. Feuillebois, & A. Sellier (Eds.), *Theoretical methods for micro scale viscous flows*. Transworld Research Network. ISBN: 978-81-7895-400-4.
Pecault, I., Gensdarmes, F., Basso, G., & Sommer, F. (2012). Performance assessment of probes dedicated to the monitoring of surface particle contamination. *Particle and Particle Systems Characterization*, *29*, 156–166.
Peressadko, A. G., Hosoda, N., & Persson, B. N. J. (2005). Influence of surface roughness on adhesion between elastic bodies. *Physical Review Letters*, *95*, 1–4.
Qian, J., & Ferro, A. (2008). Resuspension of dust particles in a chamber and associated environmental factors. *Aerosol Science and Technology*, *42*, 566–578.
Reeks, M., & Hall, D. (2001). Kinetic models for particle resuspension in turbulent flowsTheory and measurement. *Journal of Aerosol Science*, *32*, 1–31.
Rosati, J., Thornburg, J., & Rodes, C. (2008). Resuspension of particulate matter from carpet due to human activity. *Aerosol Science and Technology*, *42*, 472–482.
Soltani, M., & Ahmadi, G. (1995). Direct numerical simulation of particle entrainment in turbulent channel flow. *Physics of Fluids*, *7*, 647–657.
Soltani, M., Ahmadi, G., Bayer, R. G., & Gaynes, M. A. (1995). Particle detachment mechanisms from rough surfaces under substrate acceleration. *Journal of Adhesion Science and Technology*, *9*, 453–473.
Tan, C., Gao, S., Wee, B., Asa-Awuku, A., & Thio B. J. R. (2014). Adhesion of dust particles to common indoor surfaces in an air-conditioned environment. *Aerosol Science and Technology*, *48*, 541–551.
Valega-Mackenzie, F., & Thijsse, B.J. (2013). Atomistic modeling of alumina/epoxy adhesion. In *Symposium TT—Defects and microstructure complexity in materials. Materials research society (MRS) proceedings.* (Vol. 1526).
Vinogradova, O. I., & Feuillebois, F. (2000). Elastohydrodynamic collision of two spheres allowing slip on their surfaces. *Journal of Colloid and Interface Science*, *221*, 1–12.
Vinogradova, O., & Yakubov, G. (2006). Surface roughness and hydrodynamic boundary conditions. *Physical Review E*, *66*, 1–4.
Walker, M., Mc Farlane, J., Glasgow, D., Chung, E., Taboada-Serrano, P., Yiacoumi, S., & Tsouris, C. (2010). Influence of radioactivity on surface interaction forces. *Journal of Colloid and Interface Science*, *350*, 595–598.
Zhang, F., Reeks, M., & Kissane, M. (2013). Particle resuspension in turbulent boundary layers and the influence of non-Gaussian removal forces. *Journal of Aerosol Science*, *58*, 103–128.
Zhang, X., Ahmadi, G., Qian, J., & Ferro, A. (2008). Particle detachment, resuspension and transport due to human walking in indoor environments. *Journal of Adhesion Science and Technology*, *22*, 591–621.